



On high-order conservative finite element methods

Eduardo Abreu^a, Ciro Díaz^a, Juan Galvis^b, Marcus Sarkis^c

^aUniversity of Campinas, Department of Applied Mathematics, 13.083-970, Campinas, SP, Brazil; eabreu@ime.unicamp.br

^bDepartamento de Matemáticas, Universidad Nacional de Colombia, Bogotá D.C., Colombia.

^cDepartment of Mathematical Sciences, Worcester Polytechnic Institute Worcester USA.

Abstract

A new high-order conservative finite element method for Darcy flow is presented. The key ingredient in the formulation is a volumetric, residual-based, based on Lagrange multipliers in order to impose conservation of mass that does not involve any mesh dependent parameters. We obtain a method with high-order convergence properties with locally conservative fluxes. Furthermore, our approach can be straightforwardly extended to three dimensions. It is also applicable to highly heterogeneous problems where high-order approximation is preferred.

© 2014 Published by Elsevier Ltd.

Keywords: Conservative High-order FEM, Darcy flow, Porous media, high contrast heterogeneity, Elliptic-Poisson problem

PACS: 47.11.Df, 47.40.Nm, 47.56.+r

2000 MSC: 76S05, 76M10, 76M20

1. Problem

Many porous media related practical problems lead the numerical approximation of the pressure equation

$$-\text{div}(\Lambda(x)\nabla p) = q \quad \text{in } \Omega \subset \mathbb{R}^2, \tag{1}$$

$$p = 0 \quad \text{on } \partial\Omega. \tag{2}$$

In multi-phase immiscible incompressible flow, p and λ are the unknown pressure and the given phase mobility of one the phase in consideration (water, oil or gas); (see e.g., [4, 3, 18, 17, 1, 2]). The objective of find an approximation for p satisfying the above equation and without loss of generality we assume Dirichlet boundary conditions. In general, the forcing term q is due to gravity, sources or sinks. The mobility phase in consideration $\Lambda(x) = K(x)k_r(S(x))/\mu$, where $K(x)$ is absolute (intrinsic) permeability, k_r is the relative phase permeability and μ the phase viscosity of the fluid. Here Ω is a convex polygonal and two-dimesional domain with boundary $\partial\Omega$.

Efficiently and accurately solving the equations like (1) governing fluid flow in oil reservoirs as well as in ground-water modeling and simulation of flow linked to advective/convective transport phenomena (e.g., [21, 5]) is very challenging because of the complex porous media environment and the intricate properties of fluid phases. A key ingredient on the transport phenomena in porous media and related real-life applications is precisely the well-known Darcy law, in which linked to equations in (1), is a fundamental PDE with a wide spectrum of relevance, of fundamental applied mathematics [10, 22], fundamental of modeling fluid flow flow through porous media [21, 5] as well as of a benchmark prototype model for proof-of-concept, efficient implementation and rigorous analysis for the design and development of new finite element approaches, as the one discussed here, but also for other novel procedures, for

instance MsFEM [20], virtual finite elements [6], classical mixed finite elements [8]. Indeed, Discontinuous Galerkin (DG) formulations have become an increasingly popular way to discretize the Darcy flow equations, either in the mixed finite element DG [11] or in the stabilized mixed DG [25] framework, just to name a few of the relevance of model problem (1) from different perspectives. The field of fluid flow simulation in petroleum reservoirs [21] as well as the groundwater modeling and simulation of flow [5] linked to several transport phenomena have seen significant advances in the last few decades (see, e.g., [28, 16, 14, 13, 12, 27]) due to novel discretizations associated to the Darcy problem (1), along with the challenges in modeling: flow and transport. We emphasize the challenges in the construction of new methodologies into a reservoir simulation should have into account the following issues:

- local mass conservation properties;
- stable-fast solver, and;
- the flexibility of re-use of the novel technique into more complex models (such as to nonlinear time-dependent equations).

Also, the convergence of the method should be studied for various kinds of heterogeneities linked to flow in porous media transport problems, as such incompressible immiscible two-phase flow [4, 3, 18] and incompressible immiscible three-phase flow [17, 1, 2]; see also the references cited therein.

The impact of porous media heterogeneity on Darcy flow is very relevant. A review of studies on such topic over the recent past decades can be found in [24, 21]. Even with modern novel techniques simulation of Darcy flows through a heterogeneous porous medium with fine-scale features can be computationally expensive if the flow is fully resolved. Moreover, the unstable displacement of fluids with different viscosities, or viscous fingering provides a powerful mechanism to increase fluid-fluid interfacial area and enhance mixing that is linked to the mobility phase in consideration; (see also [15]). Thus, fast multiscale reservoir simulations using Darcy flow reduced-order models based on the model problem (1) is still up to date [23, 26].

The main goal of our work is to obtain conservative solution of the equations above when they are discretized by high order continuous piecewise polynomial spaces. The obtained solution satisfies some given set of linear restrictions (may be related to subdomains of interest). Our motivations come from the fact that in some applications it is **imperative** to have some conservative properties represented as conservations of total flux in control volumes. For instance, if v^h represents the approximation to the flux (in our case $\mathbf{q}^h = \Lambda \nabla p^h$ where p^h is the approximation of the pressure), it is required that

$$\int_{\partial V} \mathbf{q}^h \cdot \mathbf{n} = \int_V q \quad \text{for each control volume } V. \quad (3)$$

Here V is a control volume that does not cross $\partial\Omega$ from a set of control volumes of interest, and here and after \mathbf{n} is the normal vector pointing out the control volume in consideration. If some appropriate version of the total flux restriction written above holds, the method that produces such an approximation is said to be a conservative discretization.

Several schemes offer conservative discrete solutions. These schemes depend on the formulation to be approximated numerically. Among the conservative discretizations for the second order formulation the elliptic problem we mention the finite volume (FV) method, some finite difference methods and some discontinuous Galerkin methods. On the other hand, for the first order formulation or the Darcy system we have the mixed finite element methods and some hybridizable discontinuous Galerkin (HDG) methods.

In this paper, we consider methods that discretize the second order formulation (1). Working with the second order formulation makes sense especially for cases where some form of high regularity holds. Usually in these cases the equality in the second order formulation is an equality in L^2 so that, in principle, there will be no need to weaken the equality by introducing less regular spaces for the pressure as it is done in mixed formulation with L^2 pressure.

Among the methods mentioned above, and especially for second order problems, a very popular conservative discretization is the FV method. The classical FV discretization provides an approximation of the solution in the space of piecewise linear functions with respect to a triangulation while satisfying conservation of mass on elements of a dual triangulation. When the approximation of the piecewise linear space is not enough for the problem at hand, advanced approximation spaces need to be used (e.g., for problems with smooth solutions some high order approximation may

be of interest). However, in some cases, this requires a sacrifice of the conservation properties of the FV method. In this work, we design and analyze conservative solution in spaces of high order piecewise polynomials. We follow the methodology [27] that imposes the total flux restrictions by employing Lagrange multiplier technique.

We note that FV methods that use higher degree piecewise polynomials have been introduced in the literature. The fact that the dimension of the approximation spaces is larger than the number of restrictions led the researchers to design some method to select solutions: For instance, in [12, 13, 14] to introduce additional control volumes to match the number of restrictions to the number of unknowns. It is also possible to consider a Petrov-Galerkin formulation with additional test functions rather than only piecewise constant functions on the dual grid. Another approaches have been also introduced, see for instance [16] and references therein.

In this paper, we consider a Ritz formulation and construct a solution procedure that combines a continuous Galerkin-type formulation that concurrently satisfies mass conservation restrictions. We impose finite volume restrictions by using a scalar Lagrange multiplier for each restriction. This is equivalently to a constraint minimization problem where we minimize the energy functional of the equation restricted to the subspace of functions that satisfy the conservation of mass restrictions. Then, in the Ritz sense, the obtained the solution is the best among all functions that satisfy the mass conservation restriction.

Another advantage of our formulation is that the analysis can be carried out with classical tools for analyzing approximations to saddle point problems [7]. We carried out and abstract analysis and present a detailed example for the case of second order piecewise polynomials. An important finding of these paper is that we where able to obtain optimal error estimates in the H^1 norm as well as the L^2 norm. As far as we are informed, optimal L^2 approximation is obtained only for specially collocated dual meshes. The optimal L^2 approximation is obtained adding the Lagrange to the approximation p_h by an Aubin-Nitsche trick; (see [28, 9]). The L^2 bound is a theoretical advantage of using a symmetric formulation for a conservative method.

The rest of the paper is organized as follows. In Section 2 we present the Lagrange multipliers formulation or our problem. In Section 3 we introduce the saddle point approximation for which and abstract analysis is presented in Section 4. In Section 5 we present the particular cases of high-order continuous finite element spaces. For this last case we present some numerical experiments in Section 6. To close the paper we present some conclusions in Section 7.

2. Lagrange multipliers and conservation of mass

The variational formulation of problem (1) is to find $p \in H_0^1(\Omega)$ such that

$$a(p, v) = F(v) \quad \text{for all } v \in H_0^1(\Omega), \quad (4)$$

where, for $p, v \in H^1(\Omega)$, the bilinear form a is defined by

$$a(p, v) = \int_{\Omega} \Lambda(x) \nabla p(x) \nabla v(x) dx, \quad (5)$$

the functional F is defined by

$$F(v) = \int_{\Omega} q(x) v(x) dx. \quad (6)$$

In order to have a general formulation we assume that $\Lambda(x)$ in Problem (4) is uniform elliptic and bounded, however, in certain parts of the paper when regularity is required, we assume $\Lambda(x) = 1$. The Problem (4) is equivalent to the minimization problem: Find p with $(p - p_D) \in H_D^1$ and such that

$$p = \arg \min_v \mathcal{J}(v), \quad (7)$$

where the minimum is taken over v such that $v - p_D \in H_D^1$ and

$$\mathcal{J}(v) = \frac{1}{2} a(v, v) - F(v), \quad (8)$$

97 where $p_D \in H^1(\Omega)$ is any extension of p_D given on $\partial\Omega$ to Ω .

98 Let p be the solution of (4) and τ_i , $1 \leq i \leq M$, be M continuous linear functionals on $H^1(D)$. Define $m_i = \tau_i(p)$,
 99 $1 \leq i \leq M$. The problem above is equivalent to: Find $(p - p_D) \in H_D^1$ such that

$$p = \arg \min_{v \in \mathcal{W}} \mathcal{J}(v), \tag{9}$$

100 where

$$\mathcal{W} = \{v : v \in H_0^1(\Omega), \text{ and } \tau_i(v) = m_i, \quad 1 \leq i \leq M\}.$$

101 Problem (9) above can be view as Lagrange multipliers min-max optimization problem. See [7] and references therein.

102 Then, in case an approximation of p , say p^h , it is required to satisfy the constraints $\tau_i(p^h) = m_i$, $1 \leq i \leq M$, we
 103 can discretize directly the formulation (9). In particular, we can apply this approach to a set of mass conservation
 104 restrictions used in finite volume discretizations.

105 In order to deal with mass conservation properties we follow the method introduced in [27]. Before continuing
 106 with the description of the problem we introduce the meshes we are going to use in our discrete problem. Let
 107 $\tau_h = \{R_j\}_{j=1}^{N_h}$ made of elements that are triangles or squares. Here N_h is the number of elements of the triangulation.

108 We also have given a dual mesh $\tau_h^* = \{V_i\}_{i=1}^{N_h}$ where the elements are called control volumes. Figure 3 illustrate a primal
 109 and dual mesh made of squares. In general it is selected one control volume per vertex of the primal triangulation.

110 In order to ensure the mass conservation, we impose it as a restriction (by using Lagrange multipliers) in each
 111 control volume $\{V_k\}_{k=1}^{N_h}$. We mention that our formulation allows for a more general case where only few control
 112 volumes, not related to the primal triangulation, are selected.

113 Recall that we assume that each V_k is a subdomain of Ω with polygonal boundary and $1 \leq 1 \leq N_h$. If $q \in L^2$ we
 114 have that (4) is equivalent to: Find $p \in H_0^1$ and such that

$$p = \arg \min_{v \in \mathcal{W}} \mathcal{J}(v), \tag{10}$$

115 where the subset of functions that satisfy the mass conservation restrictions is defined by

$$\mathcal{W} = \left\{ v \in H_0^1(\Omega), : \int_{\partial T} -\Lambda \nabla v \cdot \mathbf{n} = \int_T q \quad \text{for all } T \in \tau_h^* \right\}.$$

116 In order to proceed we define Let $M^h = \mathbb{Q}^0(\tau_h^*)$ be the space of piece constant functions on the dual mesh τ_h^* . The
 117 Lagrange multiplier formulation of problem (9) can be written as: Find p with $(p - p_D) \in H_D^1$ and $\lambda \in M^h$ that solves,

$$\max_{\mu \in \mathbb{R}^{N_h}} \min_{v \in H_0^1(\Omega)} \mathcal{J}(v) - (\bar{a}(p, \mu) - \bar{F}(\mu)). \tag{11}$$

118 Here, the total flux bilinear form $\bar{a} : H_0^1(\Omega) \times \mathbb{R}^{M_f} \rightarrow \mathbb{R}$ is defined by

$$\bar{a}(v, \mu) = \sum_{i=1}^{N_h} \mu_i \int_{\partial V_i} \Lambda \nabla v \cdot \mathbf{n} \quad \text{for all } v \in H_0^1(\Omega), \text{ and } \mu \in M^h. \tag{12}$$

119 The functional $\bar{F} : \mathbb{R}^{M_f} \rightarrow \mathbb{R}$ is defined by

$$\bar{F}(\mu) = \sum_{i=1}^{N_h} \mu_i \int_{V_i} q \quad \text{for all } \mu \in M^h.$$

120 The first order conditions of the min-max problem above give the following saddle point problem: Find p with
 121 $p \in H_0^1(\Omega)$, and $\lambda \in M^h$ that solves,

$$\begin{aligned} a(p, v) + \bar{a}(v, \lambda) &= F(v) & \text{for all } v \in H_0^1(\Omega), \\ \bar{a}(p, \mu) &= \bar{F}(\mu) & \text{for all } \mu \in M^h. \end{aligned} \tag{13}$$

122 See for instance [7]. Note that if the exact solution of problem (7) satisfies the restrictions the in the saddle point
 123 formulation above we have $\lambda = 0$ and we get the uncoupled system

$$\begin{aligned} a(p, v) &= F(v) & \text{for all } v \in H_0^1(\Omega), \\ \bar{a}(p, \mu) &= \bar{F}(\mu) & \text{for all } \mu \in M^h. \end{aligned} \quad (14)$$

124 Also observe that the second equation above corresponds to a family of equations, one for each h , all of them having
 125 the same solution.

126 3. Discretization

127 Recall that we have introduced a primal mesh $\tau_h = \{R_j\}_{j=1}^{N_n}$ made of elements that are triangles or squares. Here
 128 N_n is the number of elements of the triangulation. We also have given a dual mesh $\tau_h^* = \{V_k\}_{k=1}^{N_n}$ where the elements
 129 are called control volumes. Figure 3 illustrate a primal and dual mesh made of squares.

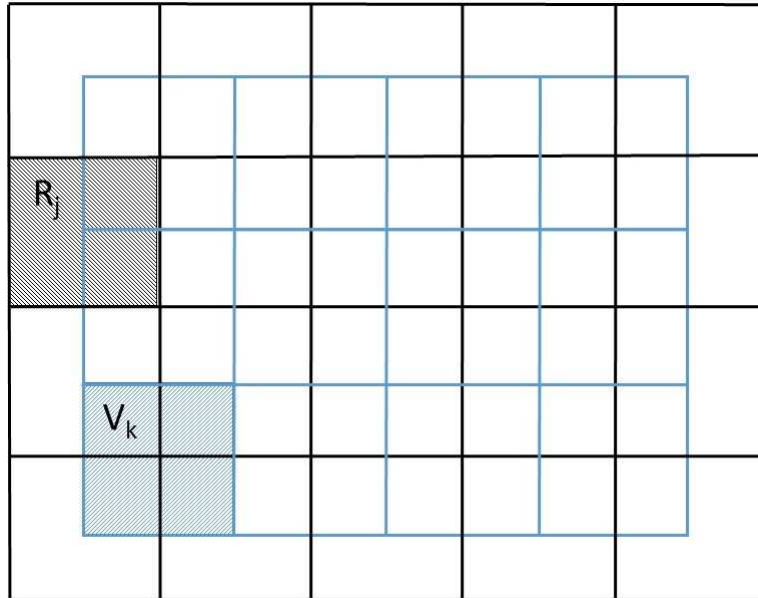


Figure 1. Example of regular mesh made of squares and its dual triangulation.

130 Let us consider $P^h = \mathbb{Q}^r(\tau_h)$ the space of continuous functions that degree polynomials of degree r on each element
 131 of the primal mesh, and $P_0^h = P^h \cap H_0^1(\Omega)$ (which are the functions in P^h that vanish in $\partial\Omega$). Let $M^h = \mathbb{Q}^0(\tau_h^*)$ be the
 132 space of piece constant functions on the dual mesh τ_h^* . We mention here that our analysis may be extended to different
 133 spaces and differential equations. See for instance [27] where we consider GMsFEM spaces instead of piecewise
 134 polynomials.

The discrete version of (15) is to find $p^h \in P^h$ and $\lambda \in M^h$ such that

$$a(p^h, v^h) + \bar{a}(v^h, \lambda^h) = F(v^h) \quad \text{for all } v^h \in P^h \quad (15)$$

$$\bar{a}(p^h, \mu^h) = \bar{F}(\mu^h) \quad \text{for all } \mu^h \in M^h. \quad (16)$$

135 Let $\{\varphi_i\}$ be the standard basis of P^h . We define the matrix

$$A = [a_{i,j}] \quad \text{where } a_{ij} = \int_{\Omega} \Lambda \nabla \varphi_i \cdot \nabla \varphi_j. \quad (17)$$

136 Note that A is the finite element stiffness matrix corresponding to finite element space P^h . Introduce also the
 137 matrix

$$\bar{A} = [\bar{a}_{k,j}] \quad \text{where } \bar{a}_{ij} = \int_{\partial V_k} \Lambda \nabla \varphi_j \cdot \mathbf{n}. \quad (18)$$

138 With this notation, the matrix form of the discrete saddle point problem is given by,

$$\begin{bmatrix} A & \bar{A}^T \\ \bar{A} & O \end{bmatrix} \begin{bmatrix} u^h \\ \lambda^h \end{bmatrix} = \begin{bmatrix} f \\ \bar{f} \end{bmatrix} \quad (19)$$

where the vector f is defined by,

$$f = [f_i] \quad \text{with } f_i = \int_{\Omega} q \cdot \varphi_i \quad \bar{f} = [\bar{f}_i]_{i=1}^{M_f} = \int_{V_k} q.$$

139 For instance, in the case of the primal and dual triangulation of Figure 3 and $r = 2$, the finite element matrix A is
 140 a sparse matrix with 19 diagonals. Also, a control volumes V_k has not empty interception with, at most, 9 supports of
 141 basis functions ϕ_j , see Figure 3. Then, matrix \bar{A} is also sparse.

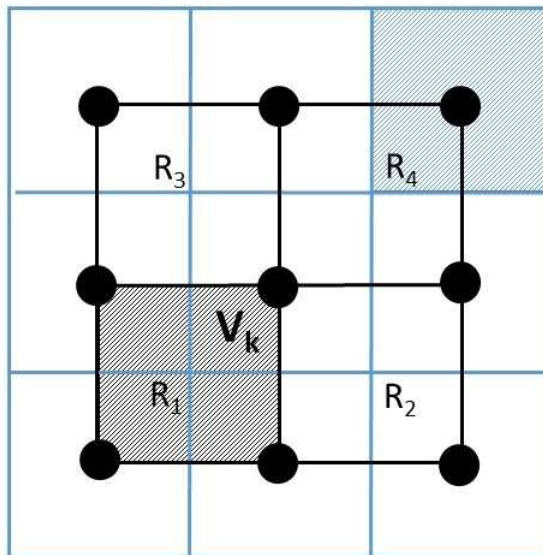


Figure 2. Control volumes that intersect the support of a \mathbb{Q}^2 basis function.

142 **Remark 1.** Note that matrix \bar{A} is related to classical (low order) finite volume matrix. Matrix \bar{A} is a rectangular
 143 matrix with more columns than rows. Several previous works on conservative high-order approximation of second
 144 order elliptic problem have been designed by “adding” rows using several constructions.

145 One can proceed as follows:

- 146 1. Construct additional control volumes and test the approximation spaces against piecewise constant functions
 147 over the total of control volumes (that include the dual grid element plus the additional control volumes).
 148 We mention that constructing additional control volumes is not an easy task and might be computationally
 149 expensive. We refer the interested reader to [12, 13, 14] for additional details.
- 150 2. Use as additional the basis functions the basis functions that correspond to nodes other than vertices to obtain
 151 an FV/Galerkin formulation. This option has the advantage that no geometrical constructions have to be carried
 152 out. On the other hand, this formulation seems difficult to analyze. Also, some preliminary numerical tests
 153 suggest that the resulting linear system becomes unstable for higher order approximation spaces (especially for
 154 the case of high-contrast multiscale coefficients).

155 3. Use the Ritz formulation with restrictions (15).

156 Note that if $r = 1$, in the linear system (19), the restriction matrix corresponds to the usual finite volume matrix.
 157 This matrix is known to be invertible. In this case, the affine space \mathcal{W}_0 is a singleton. Moreover, the only function
 158 u satisfying the restriction is given by $u = (\bar{A})^{-1}\bar{b}$. The Ritz formulation (15) reduces to the classical finite volume
 159 method.

160 Then, in the Ritz sense, the solution of (15) is not worse than any of the solutions obtained by the methods 1. or
 161 2. mentioned above. Furthermore, the solution of the associated linear system (15), which is a saddle point linear
 162 system can be readily implemented using efficient solvers for the matrix A (or efficient solvers for the classical finite
 163 volume matrix \bar{A}); See for instance [7]. Additionally, we mention that the analysis of the method can be carried out
 164 using usual tools for the analysis of restricted minimization of energy functionals and mixed finite element methods.
 165 The numerical analysis of our methodology is under current investigation and it will be presented elsewhere.

166 4. Analysis

167 We show next that imposing the conservation in control volumes using Lagrange multipliers does not interfere with
 168 the optimality of the approximation in the H^1 norm. As we will see, imposing constraints will result in non optimal
 169 L^2 approximation but we were able to reformulate the L^2 approximation to get back to the optimal approximation.

170 Recall that τ_h^* is the dual triangulation associated to the primal triangulation τ_h . In this section we assume that
 171 $\lambda\kappa = 1$ in order to simplify the notation. Let p be the solution of (4). When $f \in L^2(D)$ we have that $\nabla p \in H(\text{div}, D)$
 172 and there for p is also the pressure component of the solution of (14). We compare this solution with the the solution
 173 of the discrete problem (15).

174 In our analysis we use the energy norm in the space V and a discrete norm in the space M^h . Before proceeding we
 175 introduce notation to avoid proliferation of constants. We use the notation $A \leq B$ to indicate that there is a constant
 176 C_1 such that $A \leq C_1 B$. If additionally there exist C_2 such that $B \leq C_2 A$ we write $A \asymp B$.

177 Denote $\|v\|_a^2 = \int_{\Omega} \Lambda \nabla v \cdot \nabla v$ for all $v \in H_0^1(\Omega)$. Let us introduce the space $H := \{v \in H_0^1(\Omega) : \Lambda \nabla v \in H(\text{div}, \Omega)\}$, and
 178 set $V^h = \text{Span}\{P^h, H\}$.

180 **Assumption A:** There exist norms $\|\cdot\|_{V^h}$ and $\|\cdot\|_{M^h}$ for V^h and M^h , respectively, such that

182 1. Augmented norm: $\|v\|_a \leq \|v\|_{V^h}$ for all $v \in V$.

183 2. Continuity: there exists $|\bar{a}| \in \mathbb{R}$ such that

$$|\bar{a}(v, \mu^h)| \leq |\bar{a}| \|v\|_{V^h} \|\mu^h\|_{M^h} \quad \forall v \in V \quad \text{and} \quad \mu^h \in M^h. \quad (20)$$

184 3. Inf-Sup: there exists $\alpha > 0$ such that

$$\inf_{\mu^h \in M^h} \sup_{v^h \in P^h} \frac{\bar{a}(v^h, \mu)}{\|v^h\|_a \|\mu^h\|_{M^h}} \geq \alpha > 0. \quad (21)$$

185 **Remark 2.** The Inf-Sup condition above can be replaced by: there exists $\alpha > 0$ such that

$$\inf_{\mu^h \in M^h} \sup_{v^h \in P^h} \frac{\bar{a}(v^h, \mu)}{\|v^h\|_{V^h} \|\mu^h\|_{M^h}} \geq \alpha > 0. \quad (22)$$

186 We present a concrete example of the norms of V^h and M^h in the next section. We have the following result. The
 187 proof follows the classical approximation results of saddle point problems. We present its proof for completeness.

188 **Theorem 3.** Assume that “Assumption A” holds. Then, there exists a constant C such that

$$\|p - p^h\|_a \leq 2 \left(1 + \frac{\|\bar{a}\|}{\alpha} \right) \inf_{v^h \in P^h} \|u - v^h\|_{V^h}.$$

Proof. Note that in both problems, (14) and (15), μ_h belongs to the finite dimensional subspace M^h . Also, the exact solution of the Lagrange multiplier component of (14) is $\lambda = 0$. Now we derive error estimates following classical saddle point approximation analysis. Define

$$W^h(f) := \{v_h \in P^h : \bar{a}(v^h, \mu) = \bar{F}(\mu) \text{ for all } \mu \in M^h\}$$

and

$$W^h := \{v_h \in P^h : \bar{a}(v^h, \mu) = 0 \text{ for all } \mu \in M^h\}.$$

189 First we prove

$$\|p - p^h\|_a \leq 2 \inf_{w^h \in W^h(f)} \|p - w^h\|_a. \quad (23)$$

The inf-sup above in (21) implies that $W^h(f)$ (as well as W^h) is not empty. Take any $w^h \in W^h(f)$ and solve for z^h the problem,

$$a(v^h, z^h) = F(z^h) - a(w^h, z^h) \quad \text{for all } z^h \in V_h. \quad (24)$$

190 Since a is elliptic there exists a unique solution and therefore

$$p^h = v^h - w^h \quad (25)$$

where p^h is the solution of (15). We have from (14) and (15) and using (24) that

$$\begin{aligned} a(v^h, v^h) &= a(p^h - w^h, v^h) \\ &= a(p^h, v^h) - a(w^h, v^h) \\ &= F(v^h) - a(w^h, v^h) \\ &= a(p, v^h) - a(w^h, v^h) \\ &= a(p - w^h, v^h). \end{aligned}$$

191 Then, by using the ellipticity of a , we have

$$\|v^h\|_a^2 = a(v^h, v^h) = a(p - w^h, v^h) \leq \|p - w^h\|_a \|v^h\|_a. \quad (26)$$

Then

$$\begin{aligned} \|p - p^h\|_a &\leq \|p - w^h\|_a + \|w^h - p^h\|_a \\ &\leq \|p - w^h\|_a + \|p - w^h\|_a = 2\|p - w^h\|_a \end{aligned}$$

192 so that (23) holds true.

We now show that

$$\inf_{w^h \in W^h(f)} \|p - w^h\|_a \leq \left(1 + \frac{\|\bar{a}\|}{\alpha}\right) \inf_{v^h \in P^h} \|p - v^h\|_{V^h} \quad (27)$$

Take any $v^h \in W^h$. The inf-sup condition (21) implies that there exists a unique $z^h \in P^h$ such that

$$\bar{a}(z^h, \mu^h) = \bar{a}(p - v^h, \mu^h) \quad \text{for all } \mu^h \in M^h.$$

Then we have that $z^h \neq 0$,

$$\frac{\bar{a}(z^h, \mu^h)}{\|z^h\|_a \|\mu^h\|_{M^h}} \geq \alpha$$

and therefore

$$\begin{aligned} \|z^h\|_a &\leq \frac{1}{\alpha} \cdot \frac{\bar{a}(z^h, \mu^h)}{\|\mu^h\|} = \frac{1}{\alpha} \cdot \frac{\bar{a}(p - v^h, \mu^h)}{\|\mu^h\|_{M^h}} \\ &\leq \frac{1}{\alpha} \|\bar{a}\| \|p - v^h\|_{V^h}. \end{aligned}$$

Note that we have used the continuity of \bar{a} in the extended norm $\|\cdot\|_{V^h}$. Put $w^h = z^h + v^h$ then

$$\begin{aligned} \bar{a}(w^h, \mu^h) &= \bar{a}(z^h, \mu^h) + \bar{a}(v^h, \mu^h) \\ &= \bar{a}(p - v^h, \mu^h) + \bar{a}(v^h, \mu^h) \\ &= \bar{a}(p, \mu^h) \\ &= \bar{F}(\mu^h). \end{aligned}$$

Therefore we have that $w^h \in V_h(f)$. Moreover,

$$\begin{aligned} \|p - w^h\|_a &\leq \|p - v^h\|_a + \|v^h - w^h\|_a \\ &\leq \|p - v^h\|_a + \|z^h\|_a \\ &\leq \|p - v^h\|_a + \frac{\|\bar{a}\|}{\alpha} \cdot \|p - v^h\|_{V^h} \\ &\leq \left(1 + \frac{\|\bar{a}\|}{\alpha}\right) \|p - v^h\|_{V^h}. \end{aligned}$$

193 Combining (23) and (27) we get the result. □

194 As showed up in the numerical experiments the error $\|p - p^h\|_{L^2(D)}$ is not optimal but according to the next result
 195 if we correct p^h to $p^h + \lambda^h$ we do get optimal approximation. The proof of the following results follows a duality
 196 argument similar to that of the Aubin-Nitsche method; see [28, 9]. Since we will use regularity theorem, we will
 197 assume from now on that $\Lambda = I$ (identity). In this case, $\|\cdot\|_a = \|\cdot\|_1$, and we will show in the next section that
 198 “Assumptions A and B” hold and $1/\alpha = O(1)$ and $|\bar{a}| = O(1)$.

199 **Theorem 4.** Assume that the problem (14) is regular (see [28]) and “Assumptions A and B” hold. Then,

$$\|p - (p^h + \lambda^h)\|_{L^2(\Omega)} \leq h \|p - p^h\|_a.$$

Proof. For $g \in L^2$ define $\mathcal{S}_1^h g$ and $\mathcal{S}_0^h g$ as the solution of

$$a(\mathcal{S}_1^h g, v^h) + \bar{a}(v^h, \mathcal{S}_0^h g) = \int_D g v^h \quad \text{for all } v^h \in P^h \quad (28)$$

$$\bar{a}(\mathcal{S}_1^h g, \mu^h) = \int_D g v^h \mu^h \quad \text{for all } \mu^h \in M^h. \quad (29)$$

200 Analogously, define $S g$ as the solution of

$$\begin{aligned} a(S g, v) &= \int_D g v && \text{for all } v \in H_D^1, \\ \bar{a}(S g, \mu^h) &= \int_D g \mu^h && \text{for all } \mu^h \in M^h. \end{aligned} \quad (30)$$

201 Observe that $p^h = S_1^h q$, $\lambda^h = S_0^h q$ and $p = S q$. According to our previous result in Theorem 3 combined with standard
 202 regularity and approximation results ([28]) we have

$$\|S g - S_1^h g\|_a \leq \inf_{v^h \in P^h} \|S g - v^h\|_{V^h} \leq h \|S g\|_{H^2(\Omega)} \leq h \|g\|_{L^2(\Omega)}. \quad (31)$$

Recall that,

$$\|p - (p^h + \lambda^h)\|_{L^2(\Omega)} = \sup_{g \in L^2} \frac{(p - (p^h + \lambda^h), g)}{\|g\|_{L^2(\Omega)}}. \quad (32)$$

By using the definition of S , S_0^h and S_1^h in (28) and (30) we get

$$\begin{aligned} (p - (p^h + \lambda^h), g) &= (p, g)_0 - (p^h, g)_0 - (\lambda^h, g)_0 \\ &= a(Sg, p) - (a(S_1^h g, p^h)_0 + \bar{a}(p^h, S_0^h g)) - \bar{a}(S_1^h g, \lambda^h) \\ &= a(Sg, p) - (a(S_1^h g, p^h)_0 + \bar{a}(S_1^h g, \lambda^h)) - \bar{a}(p^h, S_0^h g) \\ &= a(Sg, p) - \left(\int_D f S_1^h g \right) - \bar{a}(p^h, S_0^h g) \\ &= a(Sg, p) - a(p, S_1^h g) - \bar{a}(p^h, S_0^h g) \\ &= a(p, Sg - S_1^h g) - \bar{a}(p^h, S_0^h g) \\ &= a(p - p^h, Sg - S_1^h g) + a(p^h, Sg - S_1^h g) - \bar{a}(p^h, S_0^h g) \\ &= a(p - p^h, Sg - S_1^h g) + a(p^h, Sg) - (a(S_1^h g, p^h) - \bar{a}(p^h, S_0^h g)) \\ &= a(p - p^h, Sg - S_1^h g) + \int_D g p^h - \left(\int_D g p^h \right) \\ &= a(p - p^h, Sg - S_1^h g) \\ &\leq \|p - p^h\|_a \|Sg - S_1^h g\|_a \\ &\leq h \|p - p^h\|_a \|g\|_{L^2(\Omega)}. \end{aligned}$$

203 In the last step we have used (31). Replacing the last inequality in (32) we get our result. □

204 5. The case of piecewise polynomials of degree two in regular meshes

205 In this section we consider a regular mesh made of squares. See Figure 3. Define

$$\Gamma^* = \bigcup_{i=1}^{N_h} \partial V_i = \bigcup_{i=1, j=1}^{N_h} (\partial V_i \cap \partial V_j)$$

that is, Γ^* is the interior interface generated by the dual triangulation. For $\mu \in M^h$ define $[\mu]$ on Γ^* as the jump across element interfaces such that $[\mu]|_{\partial V_i \cap \partial V_j} = u_i - u_j$. Note that

$$\bar{a}(p, \bar{\mu}) = \sum_{i=1}^{N_h} \mu_i \int_{\partial V_i} \nabla p \cdot \mathbf{n} = \int_{\Gamma^*} \nabla p \cdot \mathbf{n} [\mu].$$

206 For each control volume V_i , denote by $E(i)$ the set of element of the primal mesh that intersect V_i . Note that in
207 each control volume we have

$$\int_{\partial V_i} \nabla p \cdot \mathbf{n} = \sum_{\ell \in E(i)} \int_{\partial V_i \cap R_\ell} \nabla p \cdot \mathbf{n}.$$

To motivate the definition of the norms we study the continuity of the bilinear form \bar{a} . Observe that,

$$\left(\int_{\partial V_i \cap \partial V_j} \nabla p \cdot \mathbf{n} [\bar{\mu}] \right)^2 \leq \left(h \int_{\partial V_i \cap \partial V_j} (\nabla p \cdot \mathbf{n})^2 \right) \left(\frac{1}{h} \int_{\partial V_i \cap \partial V_j} [\bar{\mu}]^2 \right).$$

208 And therefore by applying Cauchy inequality and adding up we get,

$$\bar{a}(p, \bar{\mu}) \leq \left(h \int_{\Gamma^*} (\nabla p \cdot \mathbf{n})^2 \right)^{1/2} \left(\frac{1}{h} \int_{\Gamma^*} [\mu]^2 \right)^{1/2}.$$

Using an inverse inequality ([28]) we get that

$$h \int_{\Gamma^*} (\nabla p \cdot \mathbf{n})^2 = h \sum_{i=1}^{N_h} \int_{\partial V_i} (\nabla p \cdot \mathbf{n})^2 \tag{33}$$

$$= \sum_{i=1}^{N_h} \sum_{\ell \in E(i)} h \int_{\partial V_i \cap R_\ell} (\nabla p \cdot \mathbf{n})^2 \tag{34}$$

$$\leq C \sum_{i=1}^{N_h} \sum_{\ell \in E(i)} \int_{V_i \cap R_\ell} (|\nabla p|^2 + h^2 |\Delta p|^2) \tag{35}$$

$$= C \sum_{\ell=1}^{N_h} \int_{R_\ell} (|\nabla p|^2 + h^2 |\Delta p|^2) \tag{36}$$

$$= C \left(\int_D |\nabla p|^2 + h^2 \sum_{\ell=1}^{N_h} \int_{R_\ell} |\Delta p|^2 \right). \tag{37}$$

209 Now we are ready to define the norm

$$\|p\|_{V^h}^2 = |p|_{H^1(R)}^2 + h^2 \sum_{\ell=1}^{N_h} \int_{R_\ell} |\Delta p|^2 \tag{38}$$

210 Note that if $p_n \in Q_1$, the, $\|p_n\|_{V^h}^2 = |p_n|_{H^1(R)}^2$. Also, if $p_n \in Q_2$ we have, $\|p_n\|_{V^h}^2 \leq c|p_n|_{H^1(R)}^2$.

211 Also define the discrete norm for the spaces of Lagrange multipliers as

$$\|\mu\|_{M^h}^2 = \frac{1}{h} \int_{\Gamma^*} [\mu]^2. \tag{39}$$

We just showed above that the form \bar{a} is continuous, that is, there is a constant C such that,

$$\bar{a}(p, \mu_n) \leq C \|p\|_{V^h} \|\mu_n\|_{M^h}.$$

212 This also implies continuity in the H^1 norm.

213 Now let us show the inf-sup condition.

214 **Theorem 5.** Consider the norms for V^h and M^h defined in (38) and (39), respectively. There is a constant α such that,

$$\inf_{\mu \in M^h} \sup_{v^h \in Q_1} \frac{\bar{a}(v^h, \mu)}{\|v^h\|_a \|\mu\|_{M^h}} \geq \alpha > 0. \tag{40}$$

215 *Proof.* Given $\mu \in P_0$ define $v \in Q^1$ as $v(x) = \bar{\mu}(x)$ if x is a nodal point. We first verify that,

$$|v|_{H^1}^2 = \|v\|_{V^h}^2 \asymp \|\mu\|_{M^h}^2. \tag{41}$$

216 It is enough to verify this equivalence of norms in the reference square $[0, 1] \times [0, 1]$. Denote by P_i , $i = 1, 2, 3, 4$
217 the values of the function v at the nodes of the reference element. We have,

$$v = P_1(1-x)(1-y) + P_2(x)(1-y) + P_3(1-x)y + P_4xy,$$

and we can directly compute $\partial_x V_n = (P_2 - P_1)(1 - y) + (P_4 - P_3)y$ and $\partial_y V_n = (P_3 - P_1)(1 - x) + (P_4 - P_2)x$. Therefore,

$$\begin{aligned} (P_2 - P_1)^2 \frac{1}{4} + (P_4 - P_3)^2 \frac{1}{4} &\leq \int_R \partial_x v_n^2 \\ &= (P_2 - P_1)^2 \frac{1}{3} + (P_4 - P_3)^2 \frac{1}{3} + (P_2 - P_1)(P_4 - P_3) \frac{1}{6} \\ &\leq (P_2 - P_1) \frac{5}{12} + (P_4 - P_3) \frac{5}{12}. \end{aligned}$$

Analogously,

$$(P_2 - P_1)^2 \frac{1}{4} + (P_4 - P_3)^2 \frac{1}{4} \leq \int_R \partial_y v_n^2 \leq (P_2 - P_1) \frac{5}{12} + (P_4 - P_3) \frac{5}{12}.$$

This prove (41). Now we verify that

$$\int_{\Gamma^*} \nabla v \cdot \mathbf{n}[\mu] \geq \|\mu\|_{M^h}^2.$$

Observe that if R is an element of the primal triangulation, $\Gamma \cap R$ can be written as the union of four segments denoted by $\Gamma_{i,R}^*$ where $i = 4(\text{up}), 2(\text{left}), 3(\text{right}), 1(\text{down})$.

$$\begin{aligned} \int_{\Gamma_{1,R}^*} \nabla v \cdot \mathbf{n}[P_2 - P_1] &= P_2 - P_1 \int_0^{1/2} (P_2 - P_1)(1 - y) + (P_4 - P_3)y \\ &= (P_2 - P_1)^2 \frac{3}{8} + (P_2 - P_1)(P_4 - P_3) \frac{1}{4}. \end{aligned}$$

Analogously,

$$\begin{aligned} \int_{\Gamma_{2,R}^*} \nabla v \cdot \mathbf{n}[P_4 - P_3] &= (P_4 - P_3)^2 \frac{3}{8} + (P_2 - P_1)(P_4 - P_3) \frac{1}{4} \\ \int_{\Gamma_{3,R}^*} \nabla v \cdot \mathbf{n}[P_3 - P_1] &= (P_3 - P_1)^2 \frac{3}{8} + (P_3 - P_1)(P_4 - P_2) \frac{1}{4} \\ \int_{\Gamma_{4,R}^*} \nabla v \cdot \mathbf{n}[P_4 - P_2] &= (P_4 - P_2)^2 \frac{3}{8} + (P_3 - P_1)(P_4 - P_2) \frac{1}{4} \end{aligned}$$

If we add these last form equations we get

$$\int_{\Gamma^*} \nabla v \cdot \mathbf{n}[\mu] \geq (P_2 - P_1)^2 + (P_3 - P_1)^2 + (P_4 - P_2)^2 + (P_4 - P_3)^2.$$

218 This finish our proof. □

219 **Assumption B:** Let $v \in H^2(\Omega)$. Then following approximation holds

$$\inf_{v_h \in P^h} \|v - v_h\|_{V^h} \leq Ch|v|_{H^2(\Omega)}.$$

220 We mention that, for regular meshes and Q_2 finite element spaces and the norm $\|\cdot\|$ defined in (38), Assumption B
221 follows from classical finite element approximation and stability results of finite element interpolation operators. See
222 [28].

223 **Corollary 1.** Consider the norms for V^h and M^h defined in (38) and (39), respectively. If $p \in H^2(\Omega)$ and “Assumptions
224 A and B” hold, then

$$\|p - p^h\|_a \leq \inf_{v^h \in \mathbb{Q}_2} \|u - v^h\|_{V^h} \leq h|p|_{H^2(\Omega)}$$

225 and if the problem is regular

$$\|p - (p^h + \lambda_h)\|_0 \leq h\|p - p^h\|_{V^h} \leq h^2|p|_{H^2(\Omega)}.$$

226 We finish this section by mentioning that our analysis is valid for high order finite element on regular meshes made
227 of triangles since a similar analysis holds in this case.

228 6. Numerical Experiments

229 We consider the Dirichlet problem (1). We use $r = 2$ for the numerical illustration and $r = 1$ for comparison.
 230 We also employ the meshes depicted in Figure 3 with a variety of mesh sizes. We impose conservation of mass as
 231 described in the paper by using Lagrange multipliers. For this paper, we solved the saddle point linear system by LU
 232 decomposition. Several iterative solvers can be proposed for this saddle point problem but this will be considered in
 233 future studies and not here.

234 6.1. Regular case with Dirichlet's boundary condition

235 Consider $\Omega = [0, 1] \times [0, 1]$. We consider a regular mesh made of 2^M squares. The dual mesh is constructed by
 236 joining the centers of the elements of the primal mesh. We performed a series of numerical experiments to compare
 237 properties of FEM solutions with the solution of our high order FV formulation (to which we refer from now on as
 238 FV solution).

239 6.2. Smooth problem with Dirichlet boundary conditions

We selected the following forcing and exact solution,

$$q(x, y) = 2\pi(\cos(\pi x) \sin(\pi y) - 3 \sin(\pi x) \cos(\pi y) + \pi \sin(\pi x) \sin(\pi y)(-x + 3y)),$$

$$p(x, y) = \sin(\pi x) \sin(\pi y)(-x + 3y).$$

240 First we implemented the case of Q_1 elements that corresponds to the classical finite element and classical finite
 241 volume methods. We compute L^2 and H^1 errors. We present the results in Table 1 and displayed graphically in
 242 Figures 3 and 4. We observe here optimal convergence of both strategies. We mention that for this numerical test we
 243 have solved all the linear systems by using MatLab backslash operator.

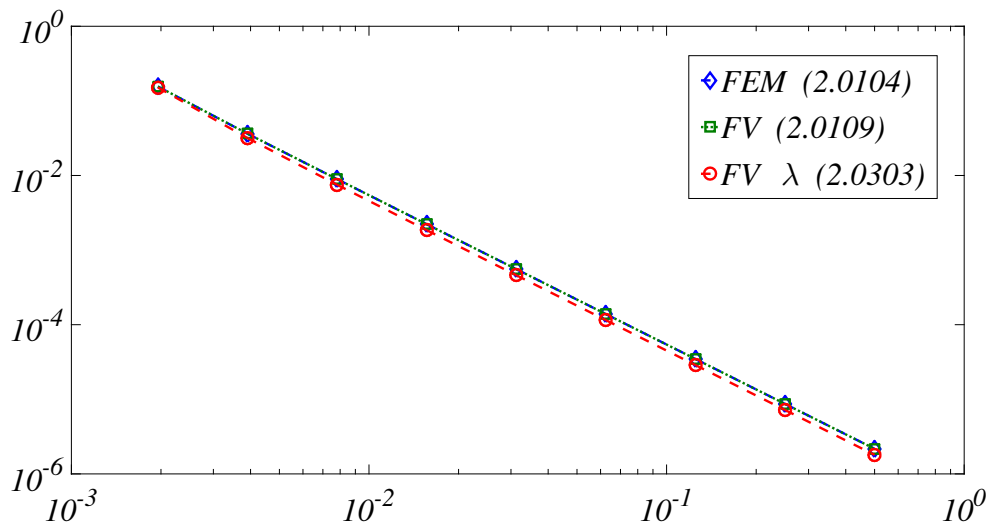


Figure 3. Log-log graphic of **FEM** and **FV** L^2 errors for numerical solutions of Example 1, using Q^1 discretization, $h = 2^{-M}$, $M = 1, \dots, 9$.

244 We now consider the case of Q_2 finite element space. We have computed the FEM solution as well as the solution
 245 of the saddle point system (15). We call this last solution the High order FV solution. We estimate the L^2 and H^1
 246 errors for both FEM and FV and compare the results through the log-log graphics shown in Figure 5 and Figure 6.
 247 See also the Table 2 for comparisons. Numerical convergence is observed with a rate of 2 for the H^1 error. The error
 248 $p - p^h$ is not optimal in L^2 . For this error, the observed convergence rate is close to 2 but if we observe the error
 249 $p - (p^h + \lambda^h)$ in L^2 we estimate a convergence rate of 3. These results coincide with our theoretical predictions four
 250 our High order FV formulation.

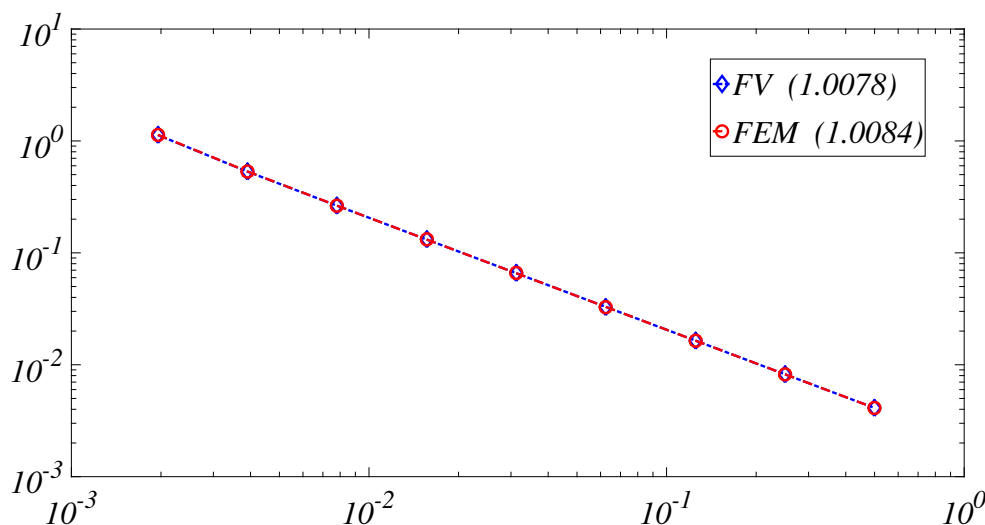


Figure 4. Log-log graphic of **FEM** and **FV** H^1 errors for numerical solutions of Example 1, using Q^1 discretization, $h = 2^{-M}$, $M = 1, \dots, 9$.

M	$FEM, L^2 Error$	$FV, L^2 Error$	$FV, H^1 Error$	$FV, H^1 Error$
1	1.5538×10^{-1}	1.5103×10^{-1}	1.1297×10^0	1.1338×10^0
2	3.6342×10^{-2}	3.1881×10^{-2}	5.3226×10^{-1}	5.3416×10^{-1}
3	8.9720×10^{-3}	$7.5.276 \times 10^{-3}$	2.6374×10^{-1}	2.6403×10^{-1}
4	2.2548×10^{-3}	1.9348×10^{-3}	1.3163×10^{-1}	1.3172×10^{-1}
5	5.5513×10^{-4}	4.6095×10^{-4}	6.5833×10^{-2}	6.5840×10^{-2}
6	1.3875×10^{-4}	1.1513×10^{-4}	3.2948×10^{-2}	3.2924×10^{-2}
7	3.4685×10^{-5}	2.8776×10^{-5}	1.6418×10^{-2}	1.6489×10^{-2}
8	8.6711×10^{-6}	7.1935×10^{-6}	8.2838×10^{-3}	8.2141×10^{-3}
9	2.1678×10^{-6}	1.7983×10^{-6}	4.1639×10^{-3}	4.1857×10^{-3}

Table 1. Table of **FEM** and **FV** L^2 and H^1 errors for numerical solutions of Example 1, using Q^1 discretization, calculated over 9 different values of mesh norm, $h = 2^{-M}$.

251 We now turn our attention to the norm $\|\cdot\|_{V^h}$, defined in (38), of the computed error. We introduce the seminorm,

$$|p|_{V^h}^2 = \sum_{\ell=1}^{N_h} \int_{R_\ell} |\Delta p|^2. \tag{42}$$

252 Note that $\|p\|_{V^h}^2 = |p|_{H^1}^2 + h^2|p|_{V^h}^2$. We present the results in Table 3. We see from this results that the error in the
 253 seminorm $|p|_{V^h}^2$ decays linearly and recall that for our result to hold it is enough this seminorm to be bounded since
 254 this term is scaled by a factor h in the definition of the extended norm (38).

255 Using our high order formulation we compute the conservative approximation of the pressure and a Lagrange
 256 multiplier which is used to correct the solution for a improved L^2 approximation. Note that the exact solution value
 257 of the Lagrange multiplier is $\lambda = 0$. We now compute the error in the Lagrange multiplier approximation. The results
 258 are presented in Table 4. We observe a convergence of order 2 in the approximation of the Lagrange multiplier.

259 To finish this subsection we compute energy and conservation of mass indicators in Table 5. The energy is defined
 260 as

$$E(p) = \frac{1}{2} \int_{\Omega} |\nabla p|^2 dx - \int_{\Omega} qp \tag{43}$$

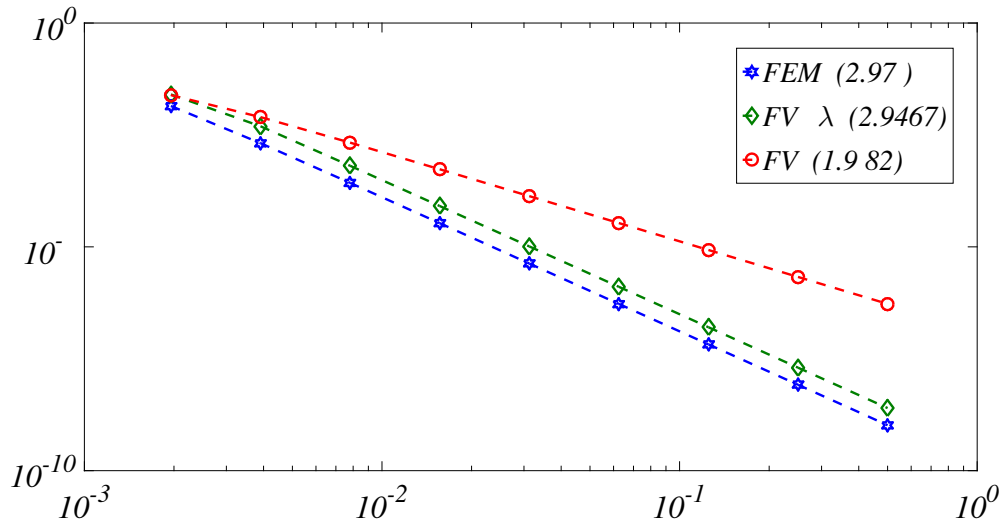


Figure 5. Log-log graphic of **FEM** and **FV** L^2 errors for numerical solutions of Example 1, using Q^2 discretization, $h = 2^{-M}$, $M = 1, \dots, 9$.

M	$FEM L^2 Error$	$FV L^2 Error$	$FEM H^1 Error$	$FV H^1 Error$
1	1.4061×10^{-2}	2.4548×10^{-2}	1.9302×10^{-1}	2.2436×10^{-1}
2	2.1217×10^{-3}	7.9336×10^{-3}	5.4862×10^{-2}	7.2895×10^{-2}
3	2.6860×10^{-4}	2.1591×10^{-3}	1.4072×10^{-2}	1.8847×10^{-2}
4	3.3875×10^{-5}	5.4159×10^{-4}	3.5418×10^{-3}	4.7552×10^{-3}
5	4.2437×10^{-6}	1.3595×10^{-4}	8.3539×10^{-4}	1.2667×10^{-3}
6	5.3075×10^{-7}	3.4023×10^{-5}	2.2016×10^{-4}	2.9616×10^{-4}
7	6.6353×10^{-8}	8.5080×10^{-6}	5.5043×10^{-5}	7.4046×10^{-5}
8	8.2944×10^{-9}	2.1271×10^{-6}	1.3761×10^{-5}	1.8512×10^{-5}
9	1.0369×10^{-9}	5.3179×10^{-7}	3.4403×10^{-6}	4.6280×10^{-6}

Table 2. Table of **FEM** and **FV** L^2 and H^1 errors for numerical solutions of Example 1, using Q^2 discretization, calculated over 9 different values of mesh norm, $h = 2^{-M}$.

261 while the conservation of mass indicator is given by,

$$J(p) = \left(\sum_R \left(\int_{\partial R} \nabla p \eta - \int_R q \right)^2 \right)^{1/2}. \tag{44}$$

262 **6.3. Problems with Neumann boundary condition**

263 For comparison, we also solve two problems with Neumann boundary conditions. The first problem has a singular
 264 forcing term in the form of a font located at (0, 0) and a source located in (1, 1). The computed solution for this
 265 problem is shown in the Figure 6.3.1. The second problem has a smooth forcing term.

266 **6.3.1. Singular forcing**

267 Table 6 shows **FEM** and **FV** computed order of convergence of the error. Apart from computing L^1 and L^2 norms
 268 of the error we also include the measure of the error in the seminorm $W^{1,1}$ (note that in this case the solution of this
 269 problems in not regular). We observe here that, in terms of approximation, the performance of both strategies **FEM**
 270 and **FV** perform similarly with respect to the order of the polynomials. The main difference between the two computed
 271 solution being only the conservation of mass that is being satisfied only by the **FV** solution.

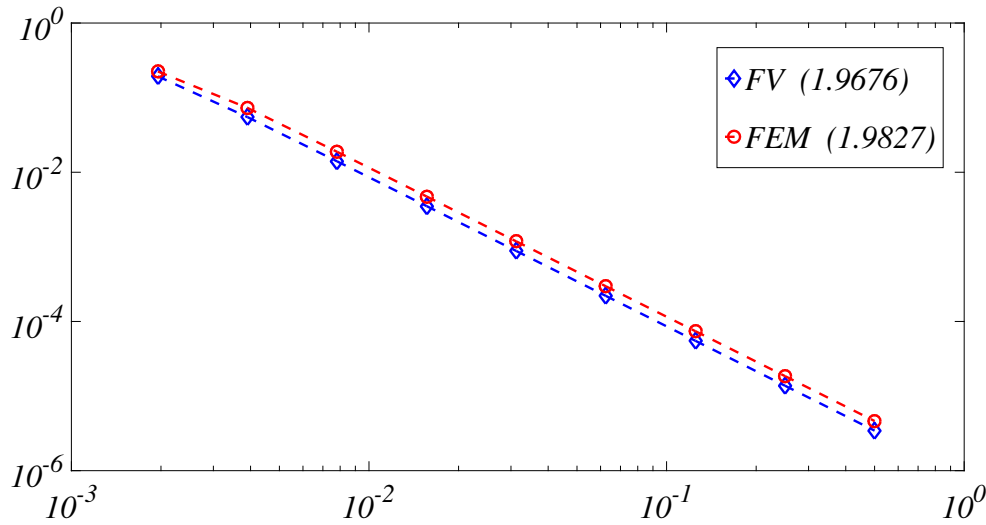


Figure 6. Log-log graphic of **FEM** and **FV** H^1 errors for numerical solutions of Example 1, using Q^2 discretization, $h = 2^{-M}$, $M = 1, \dots, 9$.

M	$ p _{V_h}^2$
1	2.9810×10^0
2	1.6915×10^0
3	8.6654×10^{-1}
4	4.3578×10^{-1}
5	2.1820×10^{-1}
6	1.0914×10^{-1}
7	5.4574×10^{-2}
8	2.7288×10^{-2}
9	1.3644×10^{-2}

Table 3. Table of scaled seminorm errors, see (42), for **FV** solution, $h = 2^{-M}$.

272 6.3.2. Smooth forcing

273 To finish our comparison with Neumann boundary condition we consider the case where the flux term is given by
 274 $q(x, y) = x - y$. In Table 7 we show the results. We obtain expected results with our FV formulation being as accurate
 275 as the FEM formulation and still satisfying the conservation of mass restrictions.

276 7. Conclusions and perspectives

277 As we previously announced, we have emphasized the challenges in the construction of new methodologies into
 278 a reservoir simulation should have into account the following issues: 1) local mass conservation properties, 2) stable-
 279 fast solver and 3) the flexibility of re-use of the novel technique into more complex models (such as to nonlinear
 280 time-dependent transport equations equation for the convection dominated transport equation). For Darcy-like model
 281 problems with very high contrasts in heterogeneity, the discretization of model (1) alone may be very hard to solve nu-
 282 merically due to a large condition number of the arising stiffness matrix. Moreover, the situation in even more intricate
 283 for modeling non trivial two- [19, 21] and three-phase [2, 1] transport convection dominated phenomena problems
 284 for flow through porous media (see also other relevant works [23, 4, 17, 5]). In addition, existence, uniqueness and
 285 regularity issues for such problems at a fine level out of reach. Thus, numerical simulation of fluid dynamics provide
 286 insight into the numerical simulation of fluid flow linked to theory, numerics and applications.

M	Error
1	2.4825×10^{-1}
2	9.9023×10^{-2}
3	2.5293×10^{-2}
4	6.3369×10^{-3}
5	1.5848×10^{-3}
6	3.9623×10^{-4}
7	9.9061×10^{-5}
8	2.4765×10^{-5}
9	6.1913×10^{-5}

Table 4. Table of error values for the Lagrange multiplier approximation.

M	$Q^1, E(u_{FEM})$	$Q^2, E(u_{FEM})$	$Q^1, E(u_{FV})$	$Q^2, E(u_{FV})$
1	-4.5230278474	-4.523568683883	-4.5230278425	-4.5233568683864
M	$Q^1, J(u_{FEM})$	$Q^2, J(u_{FEM})$	$Q^1, J(u_{FV})$	$Q^2, J(u_{FV})$
1	5.2434×10^{-6}	8.2205×10^{-8}	2.2928×10^{-14}	1.0261×10^{-13}

Table 5. Energy minimization and conservation indicator with $h = 2^{-9}$.

287 With this in mind, as a future perspective is to plug our novel high-order conservative finite element method in a
 288 numerical simulator. For the purpose of such study it is necessary to describe a coupled pressure-velocity (elliptic)
 289 and convection dominated transport (parabolic with a strong hyperbolic character) conservative solution and stable-
 290 fast algorithm to model essentially the interface capturing problems for multiphase flows where neither of the phases
 291 can be regarded as dominant. While the volume fractions (or saturation) are gained by solving the pertinent transport
 292 equations, fluid flow velocity is solved by solving the Darcy pressure problem; although the need of the pressure as
 293 primary unknown, is just the Darcy velocity that we need to plug into the convection dominated transport system.
 294 Thus, to achieve a sufficiently coupling between the volume fractions (or saturation) and the pressure-velocity, the full
 295 problem can be treated along with a fractional-step numerical procedure [2, 1]; we point out that we are aware about
 296 the very delicate issues linked to the discontinuous capillary-pressure (see [3] and the references therein); such issues
 297 must be considered no matter how is the time discretization of the convection dominated transport, namely, explicitly
 298 or implicitly. Before continuing, remember that Figure 3 illustrates a primal τ_h and dual τ_h^* mesh made of squares.

299 Thus, a feasible time marching algorithm (see, e.g. [2, 1, 19, 21]) to the full set of nonlinear differential model
 300 saturation-pressure-velocity equations is given by solving for the saturation, in hyperbolic -parabolic sub-steps, and
 301 the total Darcy velocity, in the velocity-pressure sub-steps. The approximation of elliptic pressure equation will take
 302 advantage of our high-order conservative finite element method while the transport equation can be handle by fast-
 303 accurate finite-volume method, by combining primal and dual meshes as we are using here.

304 Indeed, the fluxes (Darcy velocities) are smooth at the vertices of the cell defining the integration volume in
 305 the dual triangularization, since these vertices are located at the centers of non-staggered cells, away from the jump
 306 discontinuities along the edges. This facilitates the construction of second-order and high-order approximations linked
 307 to the hyperbolic-parabolic model problem. This also means that the pertinent spatial integrals can be approximated
 308 in a straightforward manner. For instance, the finite volume differencing [2, 1, 19], unlike upwind differencing, bypasses
 309 the need for Riemann solvers, yielding simplicity, avoiding dimensional splitting in multi-dimensional problems. In
 310 particular, such framework also allows for the extension of the scheme to hyperbolic systems by component-wise
 311 application of the scalar framework (for more details see [2, 1, 19] and the references cited therein). Moreover,
 312 at the same vertices of the integration volume, the novel high-order conservative finite element method gives the
 313 best accurate velocity field even in the presence of highly variable permeability fields, providing useful insights into
 314 the numerical simulation of fluid flow. This gives some of the benefits of staggering between primal and dual mesh
 315 triangulation by combining our novel high-order conservative finite element method with finite volume for hyperbolic-
 316 parabolic conservation laws modeling fluid flow in oil reservoirs and groundwater modeling as well as associated

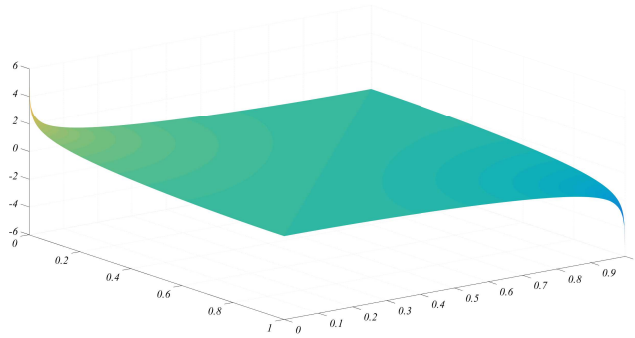


Figure 7. Plot of numerical solution for the problem with homogeneous Neumann boundary conditions and singular right hand side.

<i>FEM</i>		Q^1	Q^2
	L^1	1.8463	1.8707
	L^2	1.0000	1.0121
	$W^{1,1}$	0.8694	0.9983
<hr/>			
<i>FV</i>			
	L^1	1.8490	1.8715
	L^2	1.0000	1.0000
	$W^{1,1}$	0.8590	0.9977

Table 6. Values of L^1 , L^2 and $W^{1,1}$ error order of *FEM* and *FV* for the homogeneous Neumann boundary condition problem with singular forcing.

317 hazards of contamination and transport by ground water, CO2 geological sequestration and storage, acid mine drainage
 318 remediation, just to name a few up to date subsurface hydrology and groundwater modeling, and geothermal energy
 319 associated to petroleum science and engineering.

320 **Acknowledgements:** E. Abreu (P.I.) thanks financial support FAPESP through grants No. 2014/03204-9 and CNPq
 321 through grants No. MCTI/CNPQ/Universal 445758/2014-7. Ciro Diaz thanks CAPES for a graduate fellowship.

322 **References**

323 [1] E. Abreu, Numerical modelling of three-phase immiscible flow in heterogeneous porous media with gravitational effects, *Mathematics and*
 324 *Computers in Simulation*, 97 (2014) 234-259.
 325 [2] E. Abreu, J. Douglas, Jr., F. Furtado, D. Marchesin and F. Pereira, Three-phase immiscible displacement in heterogeneous petroleum reser-
 326 voirs. *Math. Comput. Simul.* 73(1), 2-20 (2006).
 327 [3] B. Andreianov and C. Cancs, Vanishing capillarity solutions of Buckley-Leverett equation with gravity in two-rocks medium, *Computational*
 328 *Geosciences* 17 (3) (2013) 551-572.
 329 [4] P. Bastian, A fully-coupled discontinuous Galerkin method for two-phase flow in porous media with discontinuous capillary pressure. *Comput.*
 330 *Geosci.* 18 (2014) 779-796.
 331 [5] J. Bear and C. Alexander H.-D. Cheng, *Theory and Applications of Transport in Porous Media - Modeling Groundwater Flow and Contami-*
 332 *nant Transport*, 23 Springer Science Business Media B.V. 2010.
 333 [6] L. Beirão da Veiga, F. Brezzi, L. D. Marini and A. Russo, Virtual Element Method for general second-order elliptic problems on polygonal
 334 meshes, *Math. Models Methods Appl. Sci.* 26, 729 (2016).
 335 [7] M. Benzi, G. H. Golub and J. Liesen, Numerical solution of saddle point problems, *Acta numerica* 14 (2005) 1-137.
 336 [8] D. Boffi, F. Brezzi and M. Fortin, *Mixed Finite Element Methods and Applications Vol 44* (Springer Series in Computational Mathematics),
 337 Springer Berlin Heidelberg, 2013, 685 pages.
 338 [9] D. Braess, *Finite elements (III edition) (Theory, fast solvers, and applications in elasticity theory*, Translated from the German by Larry L.
 339 Schumaker), Cambridge University Press, Cambridge 2007.
 340 [10] H. Brezis and F. Analysis, *Sobolev Spaces and Partial Differential Equations*, Springer Science Business Media, 2010, 600 pages.
 341 [11] F. Brezzi, T. J. R. Hughes, L. D. Marini, and A. Masud, A stabilized mixed discontinuous Galerkin method for Darcy flow, *Comput. Methods*
 342 *Appl. Mech. Engrg.* 195 (2006) 3347-3381.

<i>FEM</i>		Q^1	Q^2
	L^1	1.9999	3.0000
	L^2	1.9999	3.0000
	$W^{1,1}$	1.0000	2.0000
<i>FV</i>			
	L^1	2.0000	3.0000
	L^2	1.9999	3.0000
	$W^{1,1}$	1.0000	2.0000

Table 7. Values of L^1 , L^2 and $W^{1,1}$ error order of *FEM* and *FV* for the homogeneous Neumann boundary condition problem with smooth forcing.

343 [12] L. Chen, A New Class of High Order Finite Volume Methods for Second Order Elliptic Equations, *SIAM J. Numer. Anal.*, 47(6) (2010)
 344 4021-4043.

345 [13] Z. Chen, J. Wu and Y. Xu, Higher-order finite volume methods for elliptic boundary value problems, 37(2) (2012) 191-253.

346 [14] Z. Chen, Y. Xu and Y. Zhang, A construction of higher-order finite volume methods, *Math. Comp.* 84 (2015) 599-628.

347 [15] M. A. Christie and M. J. Blunt, Tenth SPE comparative solution project: a comparison of upscaling techniques. *SPE Reserv Eval Eng* 4
 348 (2001) 308-317.

349 [16] D. Cortinovis and P. Jenny, Iterative Galerkin-enriched multiscale finite-volume method, *Journal of Computational Physics*, 277(15) (2014)
 350 248-267.

351 [17] J. Dong and B. Riviere, A semi-implicit method for incompressible three-phase flow in porous media, *Comput Geosci* (DOI 10.1007/s10596-
 352 016-9583-2; First Online: 12 August 2016)

353 [18] J. Douglas Jr., F. Furtado and F. Pereira, On the numerical simulation of waterflooding of heterogeneous petroleum reservoirs, *Computational
 354 Geosciences* 1 (1997) 155-190.

355 [19] L. J. Durlofsky, A Triangle Based Mixed Finite Element-Finite Volume Technique for Modeling Two Phase Flow through Porous Media,
 356 *Journal of Computational Physics* 105(2) (1993) 252-266.

357 [20] Y. Efendiev and T. Y. Hou, *Multiscale Finite Element Methods: Theory and Applications (Surveys and Tutorials in the Applied Mathematical
 358 Sciences)* vol. 4 (2009) 234 Pages.

359 [21] M. G. Gerritsen and L. J. Durlofsky, Modeling fluid flow in oil reservoirs, *Annu. Rev. Fluid Mech.* 37 (2005) 211-38.

360 [22] D. Gilbarg and N. S. Trudinger, *Elliptic Partial Differential Equations of Second Order (Classics in Mathematics)* Springer, 2015, 518 pages.

361 [23] M. Ghasemi, Y. Yang, E. Gildin, Y. Efendiev and V. Calo, Fast multiscale reservoir simulations using POD-DEIM model reduction. Paper
 362 173271-MS presented at the SPE Reservoir Simulation Symposium, Houston, USA, 22-25 February 2015.

363 [24] G. M. Homsy, Viscous Fingering in Porous Media, *Annual Review of Fluid Mechanics*, 19 (1987) 271-311.

364 [25] T. J. R. Hughes, A. Masud and J. Wan, A stabilized mixed discontinuous Galerkin method for Darcy flow, *Comput. Methods Appl. Mech.
 365 Engrg.* 195 (2006) 3347-3381.

366 [26] J. D. Jansen and L. J. Durlofsky, Use of reduced-order models in well control optimization, *Optimization and Engineering* (First Online: 22
 367 February 2016; DOI: 10.1007/s11081-016-9313-6)

368 [27] M. Presho and J. Galvis, A mass conservative Generalized Multiscale Finite Element Method applied to two-phase flow in heterogeneous
 369 porous media, *Journal of Computational and Applied Mathematics*, 296 (2016) 376-388.

370 [28] Susanne C. Brenner and L. Ridgway Scott, *The mathematical theory of finite element methods (Texts in Applied Mathematics)* 15 3rd ed.
 371 Springer, New York 2008.



On high-order conservative finite element methods

Eduardo Abreu^a, Ciro Díaz^a, Juan Galvis^b, Marcus Sarkis^c

^aUniversity of Campinas, Department of Applied Mathematics, 13.083-970, Campinas, SP, Brazil; eabreu@ime.unicamp.br

^bDepartamento de Matemáticas, Universidad Nacional de Colombia, Bogotá D.C., Colombia.

^cDepartment of Mathematical Sciences, Worcester Polytechnic Institute Worcester USA.

Abstract

We describe and analyze a volumetric and residual-based Lagrange multipliers saddle point reformulation of the standard high-order finite method, to impose conservation of mass constraints for simulating the pressure equation on two dimensional convex polygons, with sufficiently smooth solution and mobility phase. We establish high-order a priori error estimates with locally conservative fluxes and numerical results are presented that confirm the theoretical results.

© 2014 Published by Elsevier Ltd.

Keywords: Conservative High-order FEM, Darcy flow, Porous media, high contrast heterogeneity, Elliptic-Poisson problem

PACS: 47.11.Df, 47.40.Nm, 47.56.+r

2000 MSC: 76S05, 76M10, 76M20

1. Problem

Many porous media related practical problems lead to the numerical approximation of the pressure equation

$$-\operatorname{div}(\Lambda(x)\nabla p) = q \quad \text{in } \Omega \subset \mathbb{R}^2, \quad (1)$$

$$p = 0 \quad \text{on } \partial\Omega_D, \quad (2)$$

$$\nabla p \cdot \mathbf{n} = 0 \quad \text{on } \partial\Omega \setminus \partial\Omega_D, \quad (3)$$

where $\partial\Omega_D$ is the part of the boundary of the domain Ω (denoted by $\partial\Omega$) where the Dirichlet boundary condition is imposed. In case the measure of $\partial\Omega_D$ (denoted by $|\partial\Omega_D|$) is zero, we assume the compatibility condition $\int_{\Omega} q \, dx = 0$. On the above equation we have assumed without loss of generality homogeneous boundary conditions since we can always reduce the problem to that case. The domain Ω is assumed to be a convex polygonal region in order at least H^2 regularity, see [1], and for a rectangle domain the problem is H^p regular for any integer p . We note however that this convexity or rectangularity are not required for the discretization, they are required only when regularity theory of partial differential equations (PDEs) is considered for establishing the a priori error estimates.

In multi-phase immiscible incompressible flow, p and Λ are the unknown pressure and the given phase mobility of one of the phases in consideration (water, oil or gas); (see e.g., [2, 3, 4, 5, 6, 7]). In general, the forcing term q is due to gravity, phase transitions, sources and sinks, or when we transform a nonhomogeneous boundary condition problem to a homogeneous one. The mobility phase in consideration is defined by $\Lambda(x) = K(x)k_r(S(x))/\mu$, where $K(x)$ is the absolute (intrinsic) permeability of the porous media, k_r is the relative phase permeability and μ the phase viscosity of the fluid. The assumptions required in this numerical analysis article may not in general hold for such large-scale flow models.

The main goal of our work is to obtain conservative solution of the equations above when they are discretized by high order continuous piecewise polynomial spaces. The obtained solution satisfies some given set of linear restrictions (may be related to subdomains of interest). Our motivations come from the fact that in some applications it is **imperative** to have some conservative properties represented as conservations of total flux in control volumes. For instance, if \mathbf{q}^h represents the approximation to the flux (in our case $\mathbf{q}^h = -\Lambda \nabla p^h$ where p^h is the approximation of the pressure), it is required that

$$\int_{\partial V} \mathbf{q}^h \cdot \mathbf{n} = \int_V q \quad \text{for each control volume } V. \quad (4)$$

Here V is a control volume that does not cross $\partial\Omega_D$ from a set of controls volumes of interest, and here and after \mathbf{n} is the normal vector pointing out the control volume in consideration. If some appropriate version of the total flux restriction written above holds, the method that produces such an approximation is said to be a conservative discretization.

Several schemes offer conservative discrete solutions. These schemes depend on the formulation to be approximated numerically. Among the conservative discretizations for the second the order formulation the elliptic problem we mention the finite volume (FV) method, some finite difference methods and some discontinuous Galerkin methods. On the other hand, for the first order formulation or the Darcy system we have the mixed finite element methods and some hybridizable discontinuous Galerkin (HDG) methods.

In this paper, we consider methods that discretize the second order formulation (1). Working with the second order formulation makes sense especially for cases where some form of high regularity holds. Usually in these cases the equality in the second order formulation is an equality in L^2 so that, in principle, there will be no need to weaken the equality by introducing less regular spaces for the pressure as it is done in mixed formulation with L^2 pressure.

For second order elliptic problems, a very popular conservative discretization is the finite volume (FV) method. The classical FV discretization provides an approximation of the solution in the space of piecewise linear functions with respect to a triangulation while satisfying conservation of mass on elements of a dual triangulation. When the approximation of the piecewise linear space is not enough for the problem at hand, advance approximation spaces need to be used (e.g., for problems with smooth solutions some high order approximation may be of interest). However, in some cases, this requires a sacrifice of the conservation properties of the FV method. Here in this paper, we design and analyze conservative solution in spaces of high order piecewise polynomials. We follow the methodology in [8], that imposes the total flux restrictions by employing Lagrange multiplier technique. This methodology was developed in order to apply the higher-order methods constructed in [9, 10, 11, 12] to two-phase flow problems.

We note that FV methods that use higher degree piecewise polynomials have been introduced in the literature. The fact that the dimension of the approximation spaces is larger than the number of restrictions led the researchers to design some method to select solutions: For instance, in [13, 14, 15] to introduce additional control volumes to match the number of restrictions to the number of unknowns. It is also possible to consider a Petrov-Galerkin formulation with additional test functions rather than only piecewise constant functions on the dual grid. Other approaches, have been also introduced, see for instance [16] and references therein.

In the construction of new methodologies into a reservoir simulation should have into account the following issues: 1) local mass conservation properties, 2) stable-fast solver and 3) the flexibility of re-use of the novel technique into more complex models (such as to nonlinear time-dependent transport equations equation for the convection dominated transport equation). For Darcy-like model problems with very high contrasts in heterogeneity, the discretization of Darcy-like models alone may be very hard to solve numerically due to a large condition number of the arising stiffness matrix. Moreover, the situation is even more intricate for modeling non trivial two- [17, 18] and three-phase [7, 6] transport convection dominated phenomena problems for flow through porous media (see also other relevant works [19, 2, 5, 20]). Thus, to achieve a sufficiently coupling between the volume fractions (or saturation) and the pressure-velocity, the full problem can be treated along with a fractional-step numerical procedure [7, 6]; we point out that we are aware about the very delicate issues linked to the discontinuous capillary-pressure (see [3] and the references therein). Indeed, the fluxes (Darcy velocities) are smooth at the vertices of the cell defining the integration volume in the dual triangularization, since these vertices are located at the centers of non-staggered cells, away from the jump discontinuities along the edges. This facilitates the construction of second-order and high-order approximations linked to the hyperbolic-parabolic model problem [7, 6]. This gives some of the benefits of staggering between primal and

dual mesh triangulation by combining our novel high-order conservative finite element method with finite volume for hyperbolic-parabolic conservation laws modeling fluid flow in porous media applications.

Here in this paper, we consider a Ritz formulation and construct a solution procedure that combines a continuous Galerkin-type formulation that concurrently satisfies mass conservation restrictions. We impose finite volume restrictions by using a scalar Lagrange multiplier for each restriction. This is equivalently to a constraint minimization problem where we minimize the energy functional of the equation restricted to the subspace of functions that satisfy the conservation of mass restrictions. Then, in the Ritz sense, the obtained solution is the best among all functions that satisfy the mass conservation restriction.

Another advantage of our formulation is that the analysis can be carried out with classical tools for analyzing approximations to saddle point problems [21]. We analyze the method using an abstract framework and give an example for the case of second order piecewise polynomials. An important finding of these paper is that we were able to obtain optimal error estimates in the H^1 norm as well as the L^2 norm. Our L^2 error analysis requires additional assumptions, including specially collocated dual meshes and $\Lambda = I$, and is obtained by adding the Lagrange multipliers to the approximation p_h by an Aubin-Nitsche trick [22, 23].

The rest of the paper is organized as follows. In Section 2 we present the Lagrange multipliers formulation of our problem. In Section 3 we introduce the saddle point approximation for which the analysis is presented in Section 4. In Section 5 we present the particular cases of high-order continuous finite element spaces. For this last case we present some numerical experiments in Section 6. To close the paper we present some conclusions in Section 7.

2. Lagrange multipliers and conservation of mass

Denote $H_D^1(\Omega)$ as the subspace of functions in $H^1(\Omega)$ which vanish on $\partial\Omega_D$. In case $|\partial\Omega_D| = 0$, $H_D^1(\Omega)$ is the subspace of functions in $H^1(\Omega)$ with zero average on Ω . The variational formulation of problem (1) is to find $p \in H_D^1(\Omega)$ such that

$$a(p, v) = F(v) \quad \text{for all } v \in H_D^1(\Omega), \tag{5}$$

where the bilinear form a is defined by

$$a(p, v) = \int_{\Omega} \Lambda(x) \nabla p(x) \cdot \nabla v(x) dx, \tag{6}$$

and the functional F is defined by

$$F(v) = \int_{\Omega} q(x)v(x) dx. \tag{7}$$

In order to consider a general formulation for porous media applications we let Λ be a 2×2 matrix with entries in $L^\infty(\Omega)$ in Problem (5) to be almost everywhere symmetric positive definite matrix with eigenvalues bounded uniformly from below by a positive constant, however, in certain parts of the paper when analysis and regularity theory are required, we assume $\Lambda(x) = I(\text{identity})$. The Problem (5) is equivalent to the minimization problem: Find $p \in H_D^1$ and such that

$$p = \arg \min_{v \in H_D^1(\Omega)} \mathcal{J}(v), \tag{8}$$

where

$$\mathcal{J}(v) = \frac{1}{2}a(v, v) - F(v). \tag{9}$$

In order to deal with mass conservation properties we adopt the strategy introduced in [8]. Let us introduce the meshes we are going to use in our discrete problem. Let the primal triangulation $\mathcal{T}_h = \{R_\ell\}_{\ell=1}^{N_h}$ be made of elements that are triangles or squares and let N_h be the number of elements of this triangulation. We also have a dual mesh $\mathcal{T}_h^* = \{V_k\}_{k=1}^{N_h^*}$ where the elements are called control volumes, and N_h^* is the number of control volumes. Figure 1 illustrates a primal and dual mesh made of squares when $\partial\Omega_D = \partial\Omega$, and in this case N_h^* is equal to the number of interior vertices of the primal triangulation. In general it is selected one control volume V_k per vertex of the primal triangulation when the measure $|V_k \cap \partial\Omega_D| = 0$. In case $|\partial\Omega_D| = 0$, N_h^* is the total number of vertices of the primal triangulation including the vertices on $\partial\Omega$.

In order to ensure the mass conservation, we impose it as a restriction (by using Lagrange multipliers) in each control volume $\{V_k\}_{k=1}^{N_h^*}$. We mention that our formulation allows for a more general case where only few control volumes, not necessarily related to the primal triangulation, are selected.

Let us define the linear functional $\tau_k(v) = \int_{\partial V_k} -\Lambda \nabla v \cdot \mathbf{n} ds$, $1 \leq k \leq N_h^*$. We first note $\tau_k(v)$ is not well defined for $v \in H_D^1(\Omega)$. To fix that, recall that $q \in L^2(\Omega)$, therefore, let us define the Hilbert space

$$H_{div,\Lambda}^1(\Omega) = \{v : v \in H_D^1(\Omega) \text{ and } \Lambda \nabla v \in H(\text{div}, \Omega)\}$$

with norm $\|v\|_{H_{div,\Lambda}^1(\Omega)}^2 = \|\Lambda \nabla v \cdot \nabla v\|_{L^2(\Omega)}^2 + \|\text{div}(\Lambda \nabla v)\|_{L^2(\Omega)}^2$ where the divergence is taken in the weak sense. We note that this space and norm are well-defined with the properties of Λ described above, that is, the smaller eigenvalue of $\Lambda(x)$ is uniformly bounded from below by a positive number, by using similar arguments given in [24]*Theorem 1. It is easy to see by using integration by parts with the function $z = 1$ that τ_k is a continuous linear functional on $H_{div,\Lambda}^1(\Omega)$. The integration by parts can be performed since $\|\Lambda \nabla v \cdot \nabla v\|_{L^2(V_k)}^2 + \|\text{div}(\Lambda \nabla v)\|_{L^2(V_k)}^2$ is well-defined and bounded by $\|\Lambda \nabla v \cdot \nabla v\|_{L^2(\Omega)}^2 + \|\text{div}(\Lambda \nabla v)\|_{L^2(\Omega)}^2$.

Let p be the solution of (5) and define $m_k = \tau_k(p) = \int_{V_k} q ds$, $1 \leq k \leq N_h^*$. The problem (8) is also equivalent to: Find $p \in H_{div,\Lambda}^1(\Omega)$ such that

$$p = \arg \min_{v \in \mathcal{W}} \mathcal{J}(v), \tag{10}$$

where

$$\mathcal{W} = \{v : v \in H_{div,\Lambda}^1(\Omega) \text{ such that } \tau_k(v) = m_k, \quad 1 \leq k \leq N_h^*\}.$$

Problem (10) above can be view as Lagrange multipliers min-max optimization problem. See [21] and references therein. Then, in case an approximation of p , say p_h is required to satisfy the constraints $\tau_k(p^h) = m_k$, $1 \leq k \leq N_h^*$, we can do that by discretizing directly the formulation (10). In particular, we can apply this approach to a set of mass conservation restrictions used in finite volume discretizations.

In order to proceed with the associate Lagrange formulation, we define $M^h = \mathbb{Q}^0(\mathcal{T}_h^*)$ to be the space of piecewise constant functions on the dual mesh \mathcal{T}_h^* . For $\mu \in M^h$, depending on the context, we also interpret μ as the vector $[\mu_k]_{k=1}^{N_h^*} \in \mathbb{R}^{N_h^*}$ where $\mu_k = \mu|_{V_k}$. The Lagrange multiplier formulation of problem (10) can be written as: Find $p \in H_{div,\Lambda}^1(\Omega)$ and $\lambda \in M^h$ that solve:

$$\{p, \lambda\} = \arg \max_{\mu \in M^h} \min_{v \in H_{div,\Lambda}^1(\Omega)} \mathcal{J}(v) - (\bar{a}(p, \mu) - \bar{F}(\mu)). \tag{11}$$

Here, the total flux bilinear form $\bar{a} : H_{div,\Lambda}^1(\Omega) \times M^h \rightarrow \mathbb{R}$ is defined by

$$\bar{a}(v, \mu) = \sum_{k=1}^{N_h^*} \int_{\partial V_k} -\Lambda \nabla v \cdot \mathbf{n} \mu = \sum_{k=1}^{N_h^*} \mu_k \int_{\partial V_k} -\Lambda \nabla v \cdot \mathbf{n} \quad \text{for all } v \in H_{div,\Lambda}^1(\Omega) \text{ and } \mu \in M^h. \tag{12}$$

The functional $\bar{F} : M^h \rightarrow \mathbb{R}$ is defined by

$$\bar{F}(\mu) = \sum_{i=k}^{N_h^*} \mu_k \int_{V_k} q \quad \text{for all } \mu \in M^h.$$

Note that problem (11) depends on \mathcal{T}_h^* and therefore depends on h . The first order conditions of the min-max problem above give the following saddle point problem: Find $p \in H_{div,\Lambda}^1(\Omega)$, and $\lambda \in M^h$ that solve:

$$\begin{aligned} a(p, v) + \bar{a}(v, \lambda) &= F(v) & \text{for all } v \in H_{div,\Lambda}^1(\Omega), \\ \bar{a}(p, \mu) &= \bar{F}(\mu) & \text{for all } \mu \in M^h. \end{aligned} \tag{13}$$

See for instance [21]. Note that if the exact solution of problem (8) satisfies the restrictions in the saddle point formulation above we have $\lambda = 0$ and we get the uncoupled system

$$\begin{aligned} a(p, v) &= F(v) & \text{for all } v \in H_{div,\Lambda}^1(\Omega), \\ \bar{a}(p, \mu) &= \bar{F}(\mu) & \text{for all } \mu \in M^h. \end{aligned} \tag{14}$$

Also observe that the second equation above corresponds to a family of equations, one for each triangulation parametrized by h , all of them have the same solution.

3. Discretization

Recall that we have introduced a primal mesh $\mathcal{T}_h = \{R_\ell\}_{\ell=1}^{N_h}$ made of elements that are triangles or squares. We also have given a dual mesh $\mathcal{T}_h^* = \{V_k\}_{k=1}^{N_h^*}$ where the elements are called control volumes. In order to fix ideas we assume that the number of control volumes of \mathcal{T}_h^* equals the number of free vertices of \mathcal{T}_h^* . Figure 1 illustrates a primal and dual mesh made of squares for the case $\partial\Omega_D = \partial\Omega$.

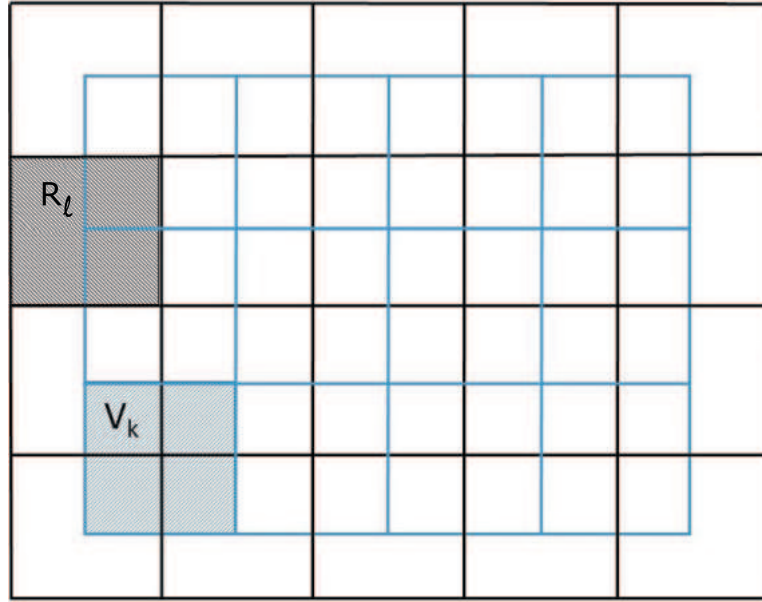


Figure 1. Example of regular mesh made of squares and its dual mesh for the case $\partial\Omega_D = \partial\Omega$.

Let us consider $P^h = \mathbb{Q}^r(\mathcal{T}_h)$ the space of continuous and piecewise polynomials of degree r on each element of the primal mesh, and $P_D^h = P^h \cap H_D^1(\Omega)$ (which are the functions in P^h that vanish in $\partial\Omega_D$). Let $M^h = \mathbb{Q}^0(\mathcal{T}_h^*)$ be the space of piecewise constant functions on the dual mesh \mathcal{T}_h^* . We mention here that our analysis may be extended to different spaces and differential equations. See for instance [8] where we consider GMSFEM spaces instead of piecewise polynomials.

The discrete version of (13) is to find $p^h \in P_D^h$ and $\lambda_h \in M^h$ such that

$$\begin{aligned} a(p^h, v^h) + \bar{a}(v^h, \lambda^h) &= F(v^h) & \text{for all } v^h \in P_D^h, \\ \bar{a}(p^h, \mu^h) &= \bar{F}(\mu^h) & \text{for all } \mu^h \in M^h. \end{aligned} \quad (15)$$

Let $\{\varphi_i\}$ be the standard basis of P_D^h . We define the matrix

$$A = [a_{i,j}] \quad \text{where } a_{ij} = \int_{\Omega} \Lambda \nabla \varphi_i \cdot \nabla \varphi_j. \quad (16)$$

Note that A is the finite element stiffness matrix corresponding to finite element space P_D^h . Introduce also the matrix

$$\bar{A} = [\bar{a}_{k,j}] \quad \text{where } \bar{a}_{k,j} = \int_{\partial V_k} -\Lambda \nabla \varphi_j \cdot \mathbf{n}. \quad (17)$$

With this notation, the matrix form of the discrete saddle point problem is given by,

$$\begin{bmatrix} A & \bar{A}^T \\ \bar{A} & O \end{bmatrix} \begin{bmatrix} p^h \\ \lambda^h \end{bmatrix} = \begin{bmatrix} f \\ \bar{f} \end{bmatrix} \quad (18)$$

where the vectors $f = [f_i]_{i=1}^{N_h}$ and $\bar{f} = [\bar{f}_k]_{k=1}^{N_h^*}$ are defined respectively by

$$f_i = \int_{\Omega} q \varphi_i \quad \text{and} \quad \bar{f}_k = \int_{V_k} q.$$

For instance, in the case of the primal and dual triangulation of Figure 2 and polynomial degree $r = 2$, the finite element matrix A is a sparse matrix with 19 diagonals. Also, for a control volume V_k there are at most 9 supports of basis functions φ_j with non-empty intersection with it, see Figure 2.

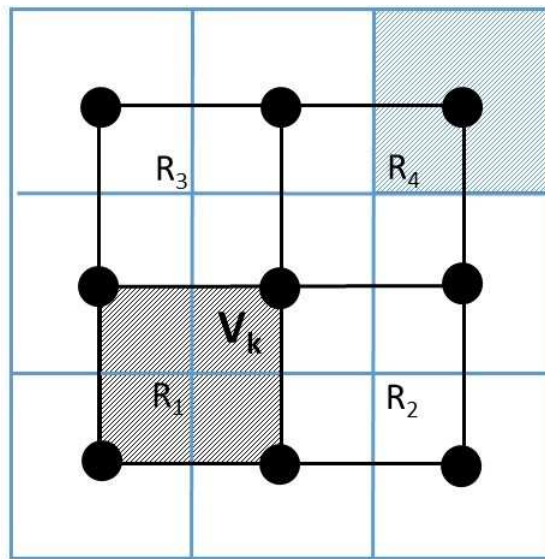


Figure 2. Control volumes that intersect the support of a $\mathbb{Q}^2(\mathcal{T}_h)$ basis function.

Remark 1. Note that matrix \bar{A} is related to classical (low order) finite volume matrix. Matrix \bar{A} is a rectangular matrix with more columns than rows. Several previous works on conservative high-order approximation of second order elliptic problem have been designed by “adding” rows using several constructions. For instance, one can proceed as follows:

1. Construct additional control volumes and test the approximation spaces against piecewise constant functions over the total of control volumes (that include the dual grid element plus the additional control volumes). We mention that constructing additional control volumes is not an easy task and might be computationally expensive. We refer the interested reader to [13, 14, 15] for additional details.
2. Use additional basis functions that correspond to nodes other than vertices to obtain an FV/Galerkin formulation. This option has the advantage that no geometrical constructions have to be carried out. On the other hand, this formulation seems difficult to analyze. Also, some preliminary numerical tests suggest that the resulting linear system becomes unstable for higher order approximation spaces (especially for the case of high-contrast multiscale coefficients).
3. Use the Ritz formulation with restrictions (15).

Note that if piecewise polynomials of degree $r = 1$ are used, in the linear system (18), the restriction matrix corresponds to the usual finite volume matrix. This matrix is known to be invertible. In this case, the affine space \mathcal{W} is a singleton. Moreover, the only function p_h satisfying the restriction is given by $p_h = (\bar{A})^{-1}\bar{f}$. The Ritz formulation (15) reduces to the classical finite volume method.

Then, in the Ritz sense, the solution of (15) is not worse than any of the solutions obtained by the method 1. or 2. mentioned above. Furthermore, the solution of the associated linear system (15), which is a saddle point linear system can be readily implemented using efficient solvers for the matrix A (or efficient solvers for the classical finite volume matrix \bar{A}); See for instance [21]. Additionally, we mention that the analysis of the method can be carried out using usual tools for the analysis of restricted minimization of energy functionals and mixed finite element methods. The numerical analysis of our methodology is under current investigation and it will be presented elsewhere.

4. Analysis

We show next that imposing the conservation in control volumes using Lagrange multipliers does not interfere with the optimality of the approximation in the H^1 norm. As we will see, imposing constraints will result in non optimal L^2 approximation but we were able to reformulate the L^2 approximation to get back to the optimal approximation by using the discrete Lagrange multiplier as a corrector.

Before proceeding we introduce notation to avoid proliferation of constants. We use the notation $A \leq B$ to indicate that there is a constant C_1 such that $A \leq C_1 B$. If additionally there exist C_2 such that $B \leq C_2 A$ we write $A \asymp B$. These constants do not depend on $\Lambda, u, u_h, \lambda_h, q$, they might depend on the shape regularity of the elements and the shape of Ω .

Denote $\|v\|_a^2 = \int_{\Omega} \Lambda \nabla v \cdot \nabla v$ for all $v \in H_D^1(\Omega)$ and let us remind that $H_{div,\Lambda}^1 := \{v \in H_D^1(\Omega) : \Lambda \nabla v \in H(\text{div}, \Omega)\}$, and set $V^h = \text{Span}\{P_D^h, H_{div,\Lambda}^1\}$. We present a concrete example of the norms of V^h and M^h in the next section, see (37) and (38), respectively.

Assumption A: There exist norms $\|\cdot\|_{V^h}$ and $\|\cdot\|_{M^h}$ for V^h and M^h , respectively, such that

1. Augmented norm: $\|v\|_a \leq \|v\|_{V^h}$ for all $v \in V^h$.
2. Continuity: there exists $\|\bar{a}\| \in \mathbb{R}$ such that

$$|\bar{a}(v, \mu^h)| \leq \|\bar{a}\| \|v\|_{V^h} \|\mu^h\|_{M^h} \quad \forall v \in V^h \quad \text{and} \quad \mu^h \in M^h. \tag{19}$$

3. Inf-Sup: there exists $\alpha > 0$ such that

$$\inf_{\mu^h \in M^h} \sup_{v^h \in P_D^h} \frac{\bar{a}(v^h, \mu)}{\|v^h\|_a \|\mu^h\|_{M^h}} \geq \alpha > 0. \tag{20}$$

Remark 2. The Inf-Sup condition above can be replaced by: there exists $\alpha > 0$ such that

$$\inf_{\mu^h \in M^h} \sup_{v^h \in P_D^h} \frac{\bar{a}(v^h, \mu)}{\|v^h\|_{V^h} \|\mu^h\|_{M^h}} \geq \alpha > 0. \tag{21}$$

We have the following result. Assume that $\{p, \lambda\}$ is the solution of (13) and $\{p_h, \lambda_h\}$ the solution of (15). We have the following result. The proof uses classical approximation techniques for saddle point problems.

Theorem 3. Assume that “Assumption A” holds. Then, there exists a constant C such that

$$\|p - p^h\|_a \leq 2 \left(1 + \frac{\|\bar{a}\|}{\alpha}\right) \inf_{v^h \in P_D^h} \|p - v^h\|_{V^h}.$$

7

Proof. Note that in both problems, (13) and (15), μ belongs to the finite dimensional subspace M^h . Also, the exact solution of the Lagrange multiplier component of (14) is $\lambda = 0$. Now we derive error estimates following classical saddle point approximation analysis. Define

$$W^h(q) := \{v_h \in P_D^h : \bar{a}(v^h, \mu) = \bar{F}(\mu) \text{ for all } \mu \in M^h\}$$

and

$$W^h := \{v_h \in P_D^h : \bar{a}(v^h, \mu) = 0 \text{ for all } \mu \in M^h\}.$$

First we prove

$$\|p - p^h\|_a \leq 2 \inf_{w^h \in W^h(q)} \|p - w^h\|_a. \quad (22)$$

The inf-sup above in (20) implies that $W^h(q)$ (as well as W^h) is not empty. Take any $w^h \in W^h(q)$ and solve for z^h the problem,

$$a(v^h, z^h) = F(z^h) - a(w^h, z^h) \quad \text{for all } z^h \in W_h. \quad (23)$$

Since a is elliptic there exists a unique solution and therefore

$$p^h = v^h - w^h, \quad (24)$$

where p^h is the solution of (15). We have from (14) and (15) and using (23) that

$$\begin{aligned} a(v^h, v^h) &= a(p^h - w^h, v^h) \\ &= a(p^h, v^h) - a(w^h, v^h) \\ &= F(v^h) - a(w^h, v^h) \\ &= a(p, v^h) - a(w^h, v^h) \\ &= a(p - w^h, v^h). \end{aligned}$$

Then, by using the ellipticity of a , we have

$$\|v^h\|_a^2 = a(v^h, v^h) = a(p - w^h, v^h) \leq \|p - w^h\|_a \|v^h\|_a. \quad (25)$$

Then

$$\begin{aligned} \|p - p^h\|_a &\leq \|p - w^h\|_a + \|w^h - p^h\|_a \\ &\leq \|p - w^h\|_a + \|p - w^h\|_a = 2\|p - w^h\|_a \end{aligned}$$

so that (22) holds true.

We now show that

$$\inf_{w^h \in W^h(q)} \|p - w^h\|_a \leq \left(1 + \frac{\|\bar{a}\|}{\alpha}\right) \inf_{v^h \in P_D^h} \|p - v^h\|_{V^h} \quad (26)$$

Take any $v^h \in W^h$. The inf-sup condition (20) implies that there exists a unique $z^h \in P_D^h$ such that

$$\bar{a}(z^h, \mu) = \bar{a}(p - v^h, \mu) \quad \text{for all } \mu \in M^h.$$

Then we have that $z^h \neq 0$,

$$\frac{\bar{a}(z^h, \mu)}{\|z^h\|_a \|\mu\|_{M^h}} \geq \alpha$$

and therefore

$$\begin{aligned} \|z^h\|_a &\leq \frac{1}{\alpha} \cdot \frac{\bar{a}(z^h, \mu)}{\|\mu^h\|} = \frac{1}{\alpha} \cdot \frac{\bar{a}(p - v^h, \mu)}{\|\mu\|_{M^h}} \\ &\leq \frac{1}{\alpha} \|\bar{a}\| \|p - v^h\|_{V^h}. \end{aligned}$$

Note that we have used the continuity of \bar{a} in the extended norm $\|\cdot\|_{V^h}$. Put $w^h = z^h + v^h$ then

$$\begin{aligned} \bar{a}(w^h, \mu) &= \bar{a}(z^h, \mu) + \bar{a}(v^h, \mu) \\ &= \bar{a}(p - v^h, \mu) + \bar{a}(v^h, \mu) \\ &= \bar{a}(p, \mu) \\ &= \bar{F}(\mu). \end{aligned}$$

Therefore we have that $w^h \in W_h(q)$. Moreover,

$$\begin{aligned} \|p - w^h\|_a &\leq \|p - v^h\|_a + \|v^h - w^h\|_a \\ &\leq \|p - v^h\|_a + \|z^h\|_a \\ &\leq \|p - v^h\|_a + \frac{\|\bar{a}\|}{\alpha} \|p - v^h\|_{V^h} \\ &\leq \left(1 + \frac{\|\bar{a}\|}{\alpha}\right) \|p - v^h\|_{V^h}. \end{aligned}$$

Combining (22) and (26) we get the result. □

From now on we assume from that $\Lambda = I$ (identity). In this case, $\|\cdot\|_a = |\cdot|_{H^1(\Omega)}$, and as we will see in Section 5 for regular meshes and $\mathbb{Q}^r(\mathcal{T}_h)$ elements that the ‘‘Assumption A’’ holds with $1/\alpha = O(1)$, $|\bar{a}| = O(1)$ with the norms V^h and M^h defined in (37) and (38), respectively. The next two Assumptions are discussed at the end of Section 5.

Assumption B: Assume that solution p of the problem (1) is in $H^{r+1}(\Omega)$ and the following approximation holds for some integer $r \leq 1$

$$\inf_{v_h \in P_D^h} \|p - v_h\|_{V^h} \leq h^r |p|_{H^{r+1}(\Omega)}.$$

As a corollary of ‘‘Assumptions A and B’’ and Lemma 3, we obtain

$$\|p - p^h\|_{V^h} \leq h^r |p|_{H^{r+1}(\Omega)}.$$

As we will show in the numerical experiments, the error $\|p - p^h\|_{L^2(D)}$ is not optimal but according to the next result if we correct p^h to $p^h + \lambda^h$ we recover the optimal approximation. The proof of the following results follows from a duality argument similar to that of the Aubin-Nitsche method; see [22, 23]. Let us introduce the following regularity assumption:

Assumption C: The problem is $H^2(\Omega)$ regular (see [22]) if for any $\tilde{q} \in L^2(\Omega)$ as a right-hand side for the problem (1), its solution \tilde{p} satisfies

$$\|\tilde{p}\|_{H^2(\Omega)} \leq \|\tilde{q}\|_{L^2(\Omega)}.$$

Theorem 4. Assume that $\Lambda = I$. Assume also that ‘‘Assumptions A, B and C’’ hold. Then,

$$\|p - (p^h + \lambda^h)\|_{L^2(\Omega)} \leq h^{r+1} |p|_{H^{r+1}(\Omega)}.$$

Proof. For $g \in L^2$ define $\mathcal{S}_1^h g$ and $\mathcal{S}_0^h g$ as the solution of

$$a(\mathcal{S}_1^h g, v^h) + \bar{a}(v^h, \mathcal{S}_0^h g) = \int_D g v^h \quad \text{for all } v^h \in H_{div,I}^1 \quad (27)$$

$$\bar{a}(\mathcal{S}_1^h g, \mu) = \int_D g v^h \mu \quad \text{for all } \mu \in M^h. \quad (28)$$

Analogously, define Sg as the solution of

$$\begin{aligned} a(Sg, v) &= \int_D gv & \text{for all } v \in H_{div, I}^1, \\ \bar{a}(Sg, \mu^h) &= \int_D g\mu^h & \text{for all } \mu^h \in M^h. \end{aligned} \quad (29)$$

Observe that $p^h = S_1^h q$, $\lambda^h = S_0^h q$ and $p = Sq$. According to our previous result in Theorem 3 combined with standard regularity and approximation results ([22]) we have

$$\|Sg - S_1^h g\|_a \leq \inf_{v^h \in P_D^h} \|Sg - v^h\|_{V^h} \leq h \|Sg\|_{H^2(\Omega)} \leq h \|g\|_{L^2(\Omega)}. \quad (30)$$

Recall that,

$$\|p - (p^h + \lambda^h)\|_{L^2(\Omega)} = \sup_{g \in L^2} \frac{(p - (p^h + \lambda^h), g)}{\|g\|_{L^2(\Omega)}}. \quad (31)$$

By using the definition of S , S_0^h and S_1^h in (27) and (29) we get

$$\begin{aligned} (p - (p^h + \lambda^h), g) &= (p, g)_0 - (p^h, g)_0 - (\lambda^h, g)_0 \\ &= a(Sg, p) - (a(S_1^h g, p^h)_0 + \bar{a}(p^h, S_0^h g)) - \bar{a}(S_1^h g, \lambda^h) \\ &= a(Sg, p) - (a(S_1^h g, p^h)_0 + \bar{a}(S_1^h g, \lambda^h)) - \bar{a}(p^h, S_0^h g) \\ &= a(Sg, p) - \left(\int_D f S_1^h g \right) - \bar{a}(p^h, S_0^h g) \\ &= a(Sg, p) - a(p, S_1^h g) - \bar{a}(p^h, S_0^h g) \\ &= a(p, Sg - S_1^h g) - \bar{a}(p^h, S_0^h g) \\ &= a(p - p^h, Sg - S_1^h g) + a(p^h, Sg - S_1^h g) - \bar{a}(p^h, S_0^h g) \\ &= a(p - p^h, Sg - S_1^h g) + a(p^h, Sg) - (a(S_1^h g, p^h) - \bar{a}(p^h, S_0^h g)) \\ &= a(p - p^h, Sg - S_1^h g) + \int_D gp^h - \left(\int_D gp^h \right) \\ &= a(p - p^h, Sg - S_1^h g) \\ &\leq \|p - p^h\|_a \|Sg - S_1^h g\|_a \\ &\leq h \|p - p^h\|_a \|g\|_{L^2(\Omega)} \end{aligned}$$

In the last step we have used (30). Replacing the last inequality in (31) and with ‘‘Assumption B’’, we get the result. \square

5. The case of piecewise polynomials of degree two in regular meshes

In this section we consider a regular mesh made of squares. See Figure 1. Define

$$\Gamma_h^* = \bigcup_{k=1}^{N_h^*} \partial V_k = \bigcup_{k, k'=1}^{N_h^*} (\partial V_k \cap \partial V_{k'})$$

that is, Γ_h^* is the interior interface generated by the dual mesh. For $\mu \in M^h$ define $[\mu]$ on Γ_h^* as the jump across element interfaces, that is, $[\mu]|_{\partial V_k \cap \partial V_{k'}} = \mu_k - \mu_{k'}$. Note that for $p \in V^h$

$$\bar{a}(p, \mu) = \sum_{k=1}^{N_h^*} \mu_k \int_{\partial V_k} -\nabla p \cdot \mathbf{n} = \int_{\Gamma_h^*} -\nabla p \cdot \mathbf{n} [\mu].$$

For each control volume V_k , denote by $E(k)$ the set of element of the primal mesh that intersect V_k . Note that in each control volume we have

$$\int_{\partial V_k} -\nabla p \cdot \mathbf{n} = \sum_{\ell \in E(k)} \int_{\partial V_k \cap R_\ell} -\nabla p \cdot \mathbf{n}.$$

To motivate the definition of the norms we study the continuity of the bilinear form \bar{a} . Observe that,

$$\left(\int_{\partial V_k \cap \partial V_{k'}} -\nabla p \cdot \mathbf{n} [\mu] \right)^2 \leq \left(h \int_{\partial V_k \cap \partial V_{k'}} (\nabla p \cdot \mathbf{n})^2 \right) \left(\frac{1}{h} \int_{\partial V_k \cap \partial V_{k'}} [\mu]^2 \right).$$

And therefore by applying Cauchy inequality and adding up we get,

$$|\bar{a}(p, \mu)| \leq \left(h \int_{\Gamma_h^*} (\nabla p \cdot \mathbf{n})^2 \right)^{1/2} \left(\frac{1}{h} \int_{\Gamma_h^*} [\mu]^2 \right)^{1/2}.$$

Using a trace inequality we get that

$$h \int_{\Gamma_h^*} (\nabla p \cdot \mathbf{n})^2 = h \sum_{k=1}^{N_h^*} \int_{\partial V_k} (\nabla p \cdot \mathbf{n})^2 \quad (32)$$

$$= \sum_{k=1}^{N_h^*} \sum_{\ell \in E(k)} h \int_{\partial V_k \cap R_\ell} (\nabla p \cdot \mathbf{n})^2 \quad (33)$$

$$\leq \sum_{k=1}^{N_h^*} \sum_{\ell \in E(k)} \left(|p|_{H^1(V_k \cap R_\ell)}^2 + h^2 (\|p_{xx}\|_{L^2(V_k \cap R_\ell)}^2 + \|p_{yy}\|_{L^2(V_k \cap R_\ell)}^2) \right) \quad (34)$$

$$= \sum_{\ell=1}^{N_h} \left(|p|_{H^1(R_\ell)}^2 + h^2 (\|p_{xx}\|_{L^2(R_\ell)}^2 + \|p_{yy}\|_{L^2(R_\ell)}^2) \right) \quad (35)$$

$$= |p|_{H^1(\Omega)}^2 + h^2 \sum_{\ell=1}^{N_h} (\|p_{xx}\|_{L^2(R_\ell)}^2 + \|p_{yy}\|_{L^2(R_\ell)}^2). \quad (36)$$

Now we are ready to define the norm

$$\|p\|_{V^h}^2 = |p|_{H^1(\Omega)}^2 + h^2 \sum_{\ell=1}^{N_h} (\|p_{xx}\|_{L^2(R_\ell)}^2 + \|p_{yy}\|_{L^2(R_\ell)}^2) \quad (37)$$

Note that if $p \in \mathbb{Q}^1(\mathcal{T}_h)$ then $\|p\|_{V^h}^2 = |p|_{H^1(\Omega)}^2$. Also, if $p \in \mathbb{Q}^2(\mathcal{T}_h)$ we have $\|p\|_{V^h}^2 \leq c|p|_{H^1(\Omega)}^2$ by using inverse inequality.

Also define the discrete norm for the spaces of Lagrange multipliers as

$$\|\mu\|_{M^h}^2 = \frac{1}{h} \int_{\Gamma_h^*} [\mu]^2. \quad (38)$$

We have shown above that the form \bar{a} is continuous, that is, there is a constant $|\bar{a}|$ such that,

$$|\bar{a}(p, \mu)| \leq |\bar{a}| \|p\|_{V^h} \|\mu\|_{M^h}.$$

This also implies continuity in the H^1 norm. Now let us show the inf-sup condition.

Theorem 5. Consider the norms for $\|\cdot\|_a = |\cdot|_{H^1(\Omega)}$ and M^h defined in (38), respectively. There is a constant α such that,

$$\inf_{\mu \in M^h} \sup_{v^h \in \mathbb{Q}^1(\mathcal{T}_h)} \frac{\bar{a}(v^h, \mu)}{\|v^h\|_a \|\mu\|_{M^h}} \geq \alpha > 0. \quad (39)$$

Proof. Given $\mu \in M^h$ define $v \in \mathbb{Q}^1(\mathcal{T}_h)$ as $v(x_i) = \bar{\mu}(x_i)$ if x_i is a vertex of the primal mesh in V_i and $v(x_i) = 0$ if x_i is a vertex of the primal mesh on $\partial\Omega_D$. We first verify that,

$$|v|_{H^1}^2 = \|v\|_{V^h}^2 \approx \|\mu\|_{M^h}^2. \quad (40)$$

It is enough to verify this equivalence of norms in the reference square $\hat{R} = [0, 1] \times [0, 1]$. Denote by $P_i, i = 1, 2, 3, 4$ the values of the reference function \hat{v} at the nodes of the reference element. We have,

$$\hat{v} = P_1(1-x)(1-y) + P_2(x)(1-y) + P_3(1-x)y + P_4xy,$$

and we can directly compute $\partial_x \hat{v} = (P_2 - P_1)(1-y) + (P_4 - P_3)y$ and $\partial_y \hat{v} = (P_3 - P_1)(1-x) + (P_4 - P_2)x$. Therefore, after some calculations we obtain

$$\begin{aligned} (P_2 - P_1)^2 \frac{1}{6} + (P_4 - P_3)^2 \frac{1}{6} &\leq (P_2 - P_1)^2 \frac{1}{3} + (P_4 - P_3)^2 \frac{1}{3} - |(P_2 - P_1)(P_4 - P_3)| \frac{1}{3} \\ &\leq \int_{\hat{R}} (\partial_x \hat{v})^2 \\ &\leq (P_2 - P_1)^2 \frac{1}{3} + (P_4 - P_3)^2 \frac{1}{3} + |(P_2 - P_1)(P_4 - P_3)| \frac{1}{3} \\ &\leq (P_2 - P_1)^2 \frac{1}{2} + (P_4 - P_3)^2 \frac{1}{2}. \end{aligned}$$

Analogously,

$$(P_3 - P_1)^2 \frac{1}{6} + (P_4 - P_2)^2 \frac{1}{6} \leq \int_R (\partial_y \hat{v})^2 \leq (P_3 - P_1)^2 \frac{1}{2} + (P_4 - P_2)^2 \frac{1}{2}.$$

This prove (40). Now we verify that

$$\int_{\Gamma_h^*} \nabla v \cdot \mathbf{n}[\mu] \geq \|\mu\|_{M^h}^2.$$

Observe that if R is an element of the primal triangulation, $\Gamma_h^* \cap R$ can be written as the union of four segments denoted by $\Gamma_{i,R}^*$ where $i = 4(\text{up}), 2(\text{left}), 3(\text{right}), 1(\text{down})$. Working again on the reference square, we have

$$\begin{aligned} \int_{\hat{\Gamma}_{1,\hat{R}}^*} \nabla \hat{v} \cdot \mathbf{n}[P_2 - P_1] &= (P_2 - P_1) \int_0^{1/2} (P_2 - P_1)(1-y) + (P_4 - P_3)y \\ &= (P_2 - P_1)^2 \frac{3}{8} + (P_2 - P_1)(P_4 - P_3) \frac{1}{8}. \end{aligned}$$

Analogously,

$$\begin{aligned} \int_{\hat{\Gamma}_{2,\hat{R}}^*} \nabla \hat{v} \cdot \mathbf{n}[P_4 - P_3] &= (P_4 - P_3)^2 \frac{3}{8} + (P_2 - P_1)(P_4 - P_3) \frac{1}{8} \\ \int_{\hat{\Gamma}_{3,\hat{R}}^*} \nabla \hat{v} \cdot \mathbf{n}[P_3 - P_1] &= (P_3 - P_1)^2 \frac{3}{8} + (P_3 - P_1)(P_4 - P_2) \frac{1}{8} \\ \int_{\hat{\Gamma}_{4,\hat{R}}^*} \nabla \hat{v} \cdot \mathbf{n}[P_4 - P_2] &= (P_4 - P_2)^2 \frac{3}{8} + (P_3 - P_1)(P_4 - P_2) \frac{1}{8} \end{aligned}$$

If we add these last form equations we get

$$\int_{\Gamma_h^* \cap R} \nabla v \cdot \mathbf{n}[\mu] \geq (P_2 - P_1)^2 + (P_3 - P_1)^2 + (P_4 - P_2)^2 + (P_4 - P_3)^2.$$

This finish our proof. □

We mention that for quasi-uniform and shape regular meshes, for quadrilateral $\mathbb{Q}^r(\mathcal{T}_h)$ or triangular $\mathbb{P}^r(\mathcal{T}_h)$ finite element spaces, the “Assumption B” holds for $p \in H^{r+1}(\Omega)$. For the solution p of problem (1) to be in $H^{r+1}(\Omega)$, it is necessary to impose conditions on the shape and smoothness of domain as well as on the type of boundary conditions (Dirichlet, Neumann or mixed); see [1]. For instance, for the pure homogeneous Dirichlet boundary condition case, it is sufficient that Ω be convex and $q \in L^2(\Omega)$ in order that $p \in H^2(\Omega)$, and also “Assumption C” follows. For p to be in $H^{r+1}(\Omega)$ for integer $r \leq 2$, it is sufficient that Ω be a rectangular domain and $q \in H^{r-1}(\Omega)$. Higher-order approximation and regularity can also be obtained for curved isoparametric finite elements on domains with smooth boundaries.

6. Numerical Experiments

We consider the Dirichlet problem (1) and employ the meshes depicted in Figure 1 with a variety of mesh sizes and $\Lambda = I$. We impose conservation of mass as described in the paper by using Lagrange multipliers. For this paper, we solved the saddle point linear system by LU decomposition. Several iterative solvers can be proposed for this saddle point problem but this will be considered in future studies, not here.

Consider $\Omega = [0, 1] \times [0, 1]$ and $\Lambda = I$. We consider a regular mesh made of $2^M \times 2^M$ squares. The dual mesh is constructed by joining the centers of the elements of the primal mesh. We performed a series of numerical experiments to compare properties of FEM solutions with the solution of our high order FV formulation (to which we refer from now on as FV solution). The FV formulation with correction we denote by FV + λ .

6.1. Smooth problem with nonhomogeneous Dirichlet boundary conditions

We selected the following forcing term and Dirichlet boundary conditions as

$$q(x, y) = 2\pi(\cos(\pi x) \sin(\pi y) - 3 \sin(\pi x) \cos(\pi y) + \pi \sin(\pi x) \sin(\pi y)(-x + 3y)),$$

$$u_D(x, y) = 1 + x + 2y,$$

and see that the exact solution is

$$p(x, y) = \sin(\pi x) \sin(\pi y)(-x + 3y) + 1 + x + 2y.$$

First we implemented the case of $\mathbb{Q}^1(\mathcal{T}_h)$ elements that corresponds to the classical finite element and classical finite volume methods. We compute L^2 and H^1 errors. We present the results in Table 1 and displayed graphically in Figures 3 and 4. We observe here optimal convergence of both strategies.

M	FEM, L^2 Error	FV + λ , L^2 Error	FEM, H^1 Error	FV, H^1 Error
1	1.5538×10^{-1}	1.5103×10^{-1}	1.1297×10^0	1.1338×10^0
2	3.6342×10^{-2}	3.1881×10^{-2}	5.3226×10^{-1}	5.3416×10^{-1}
3	8.9720×10^{-3}	$7.5.276 \times 10^{-3}$	2.6374×10^{-1}	2.6403×10^{-1}
4	2.2548×10^{-3}	1.9348×10^{-3}	1.3163×10^{-1}	1.3172×10^{-1}
5	5.5513×10^{-4}	4.6095×10^{-4}	6.5833×10^{-2}	6.5840×10^{-2}
6	1.3875×10^{-4}	1.1513×10^{-4}	3.2948×10^{-2}	3.2924×10^{-2}
7	3.4685×10^{-5}	2.8776×10^{-5}	1.6418×10^{-2}	1.6489×10^{-2}
8	8.6711×10^{-6}	7.1935×10^{-6}	8.2838×10^{-3}	8.2141×10^{-3}
9	2.1678×10^{-6}	1.7983×10^{-6}	4.1639×10^{-3}	4.1857×10^{-3}

Table 1. Table of FEM and FV L^2 and H^1 errors for numerical solutions of Example 1, using $\mathbb{Q}^1(\mathcal{T}_h)$ discretization, calculated over 9 different values of mesh norm, $h = 2^{-M}$.

We now consider the case of $\mathbb{Q}^2(\mathcal{T}_h)$ finite element space. We have computed the FEM solution as well as the solution of the saddle point system (15). We call this last solution the High order FV solution. We estimate the L^2 and H^1 errors for both FEM and FV and compare the results through the log-log graphics shown in Figure 5 and Figure 6. See also the Table 2 for comparisons. Numerical convergence is observed with a rate of 2 for the H^1 error. The error $p - p^h$ is not optimal in L^2 . For this error, the observed convergence rate is close to 2 but if we observe the error $p - (p^h + \lambda^h)$ in L^2 we estimate a convergence rate of 3. These results coincide with our theoretical predictions four our High order FV formulation.

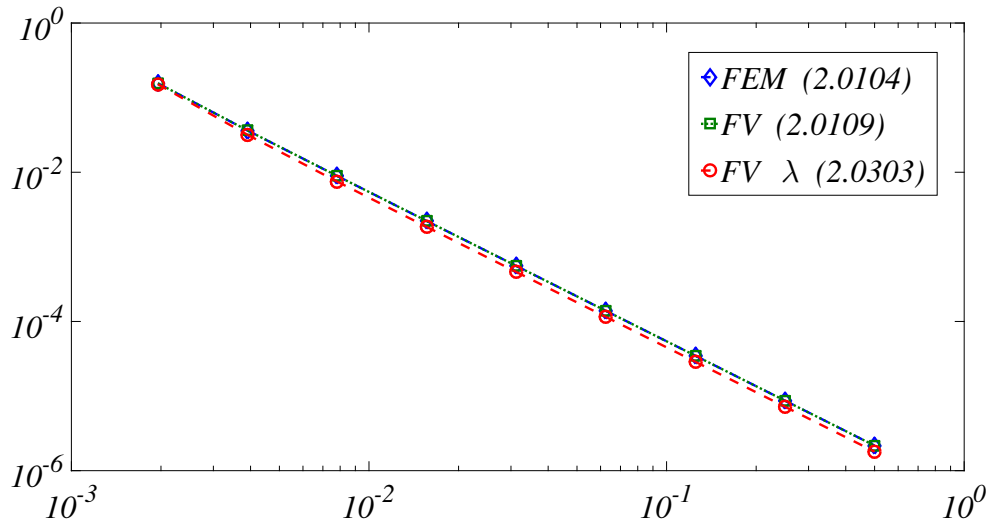


Figure 3. Log-log graphic of **FEM** and **FV** L^2 errors for numerical solutions of Example 1, using $\mathbb{Q}^1(\mathcal{T}_h)$ discretization, $h = 2^{-M}$, $M = 1, \dots, 9$.

M	$FEM L^2 Error$	$FV + \lambda, L^2 Error$	$FEM H^1 Error$	$FV, H^1 Error$
1	1.4061×10^{-2}	2.5448×10^{-2}	1.9302×10^{-1}	2.2436×10^{-1}
2	2.1217×10^{-3}	4.9023×10^{-3}	5.4862×10^{-2}	7.2895×10^{-2}
3	2.6860×10^{-4}	6.4789×10^{-4}	1.4072×10^{-2}	1.8847×10^{-2}
4	3.3875×10^{-5}	8.1756×10^{-5}	3.5418×10^{-3}	4.7552×10^{-3}
5	4.2437×10^{-6}	1.0242×10^{-5}	8.3539×10^{-4}	1.2667×10^{-3}
6	5.3075×10^{-7}	1.2810×10^{-6}	2.2016×10^{-4}	2.9616×10^{-4}
7	6.6353×10^{-8}	1.6015×10^{-7}	5.5043×10^{-5}	7.4046×10^{-5}
8	8.2944×10^{-9}	2.0019×10^{-8}	1.3761×10^{-5}	1.8512×10^{-5}
9	1.0369×10^{-9}	2.5024×10^{-9}	3.4403×10^{-6}	4.6280×10^{-6}

Table 2. Table of **FEM** and **FV** L^2 and H^1 errors for numerical solutions of Example 1, using $\mathbb{Q}^2(\mathcal{T}_h)$ discretization, calculated over 9 different values of mesh norm, $h = 2^{-M}$.

We now turn our attention to the norm $\|\cdot\|_{V^h}$, defined in (37), of the computed error. We introduce the seminorm,

$$|p|_{V^h}^2 = \sum_{\ell=1}^{N_h} \left(\|p_{xx}\|_{L^2(R_\ell)}^2 + \|p_{yy}\|_{L^2(R_\ell)}^2 \right) \tag{41}$$

Note that $\|p\|_{V^h}^2 = |p|_{H^1}^2 + h^2|p|_{V^h}^2$. We present the results in Table 3. We see from this results that the error in the seminorm $|\cdot|_{V^h}$ decays linearly with h and recall that this seminorm is scaled by a factor h in the definition of the extended norm $\|\cdot\|_{V^h}$ in (37).

Using our high order formulation we compute the conservative approximation of the pressure and a Lagrange multiplier which is used to correct the solution for a improved L^2 approximation. Note that the exact solution value of the Lagrange multiplier is $\lambda = 0$. We now compute the error in the Lagrange multiplier approximation in the M_h norm. The results are presented in Table 4. We observe a convergence of order 2 in the approximation of the Lagrange multiplier.

To finish this subsection we compute energy and conservation of mass indicators in Table 5. The energy is defined as

$$E(p) = \frac{1}{2} \int_{\Omega} |\nabla p|^2 dx - \int_{\Omega} qp \tag{42}$$

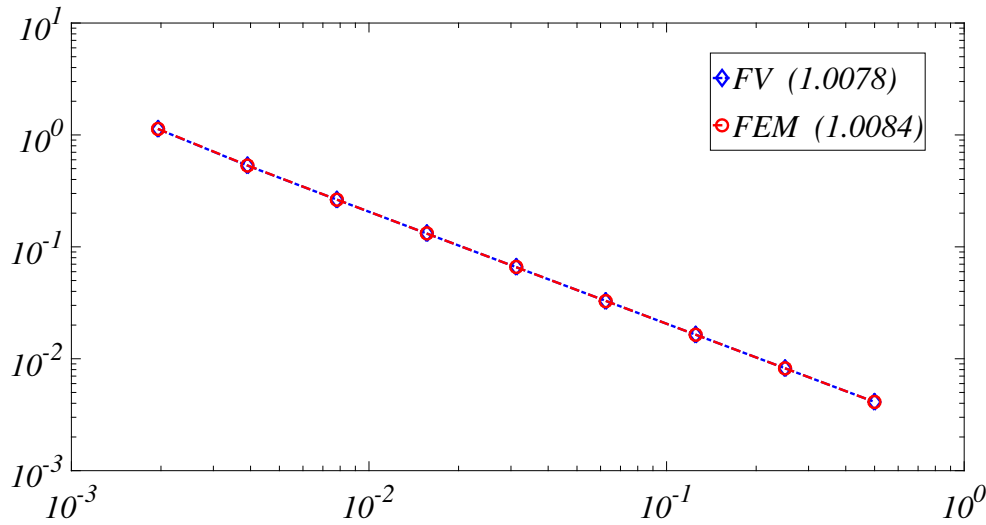


Figure 4. Log-log graphic of **FEM** and **FV** H^1 errors for numerical solutions of Example 1, using $\mathbb{Q}^1(\mathcal{T}_h)$ discretization, $h = 2^{-M}$, $M = 1, \dots, 9$.

M	$ p - p^h _{V^h}$
1	3.6040×10^0
2	1.8127×10^0
3	9.0885×10^{-1}
4	4.5506×10^{-1}
5	2.2769×10^{-1}
6	1.1388×10^{-1}
7	5.6954×10^{-2}
8	2.8480×10^{-2}
9	1.4240×10^{-2}

Table 3. Table of scaled seminorm errors, see (41), for **FV** solution, $h = 2^{-M}$. Recall that the seminorm $|\cdot|_{V^h}$ in (41) is scaled by a factor h in the definition of the extended norm (37)

while the conservation of mass indicator is given by,

$$J(p) = \left(\sum_R \left(\int_{\partial R} -\nabla p \cdot \mathbf{n} - \int_R q \right)^2 \right)^{1/2}. \tag{43}$$

6.2. Singular forcing with nonhomogeneous Neumann boundary condition

For comparison, we also solve two problems with Neumann boundary conditions. The first problem has a singular forcing term in the form of a font located at $(0, 0)$ and a source located in $(1, 1)$. The computed solution for this problem is shown in the Figure 7. The second problem has a smooth forcing term.

Table 6 shows *FEM* and *FV* computed order of convergence of the error. Apart from computing L^1 and L^2 norms of the error we also include the measure of the error in the seminorm $W^{1,1}$ (note that in this case the solution of this problems in not regular and is not in $H^1(\Omega)$). We observe here that, in terms of approximation, the performance of both strategies *FEM* and *FV* perform similarly with respect to the order of the polynomials. The main difference between the two computed solution is only the conservation of mass that is being satisfied only by the *FV* solution.

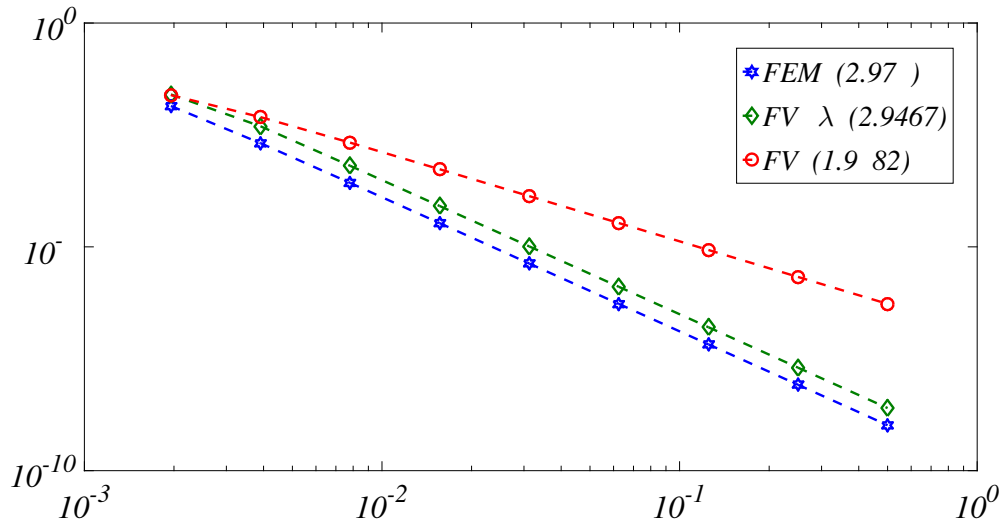


Figure 5. Log-log graphic of **FEM** and **FV** L^2 errors for numerical solutions of Example 1, using $\mathbb{Q}^2(\mathcal{T}_h)$ discretization, $h = 2^{-M}$, $M = 1, \dots, 9$.

M	Error
1	2.4825×10^{-1}
2	9.9023×10^{-2}
3	2.5293×10^{-2}
4	6.3369×10^{-3}
5	1.5848×10^{-3}
6	3.9623×10^{-4}
7	9.9061×10^{-5}
8	2.4765×10^{-5}
9	6.1913×10^{-5}

Table 4. Table of error values $\|\lambda_h - \lambda\|_{M_h}$ for the Lagrange multiplier approximation.

6.2.1. Smooth forcing

To finish our comparison with Neumann boundary condition we consider the case where the flux term is given by $q(x, y) = x - y$. In Table 7 we show the results. We obtain expected results with our FV formulation being as accurate as the FEM formulation and still satisfying the conservation of mass restrictions.

7. Conclusions

In this paper, we introduce a high-order discretization with locally conservative properties for a second-order problem. Our formulation discretizes the second order problem and there is no need to write an equivalent first order system of differential equations. It is, therefore, a novel approach and it is fundamentally different from classical mixed finite element methods such as discretizing by Raviart-Thomas elements. We impose the conservative constraints by using a Lagrange multiplier for each control volume and therefore we can compute locally conservative solutions while keeping the high-order approximation. For the case of constant permeability coefficient, we present the analysis of our formulation at the continuous and discrete levels. In particular, we obtain optimal estimates for the H^1 and L^2 norms. We mention also that the optimal L^2 approximation is obtained without any post-processing or hybridization which are other differences with classical mixed finite element methods. The analysis can be straightforwardly extended to the case of smooth permeability coefficients.

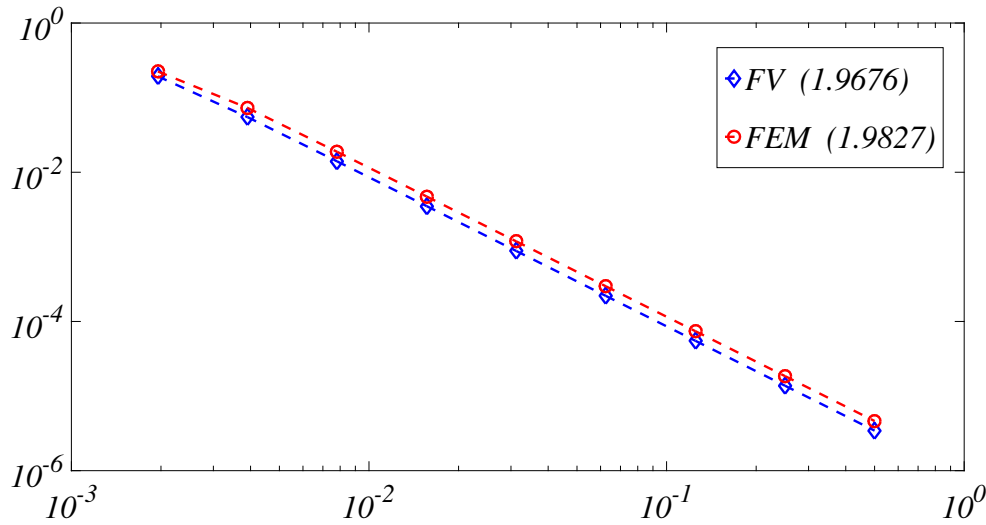


Figure 6. Log-log graphic of **FEM** and **FV** H^1 errors for numerical solutions of Example 1, using $\mathbb{Q}^2(\mathcal{T}_h)$ discretization, $h = 2^{-M}$, $M = 1, \dots, 9$.

M	$\mathbb{Q}^1, E(u_{FEM})$	$\mathbb{Q}^2, E(u_{FEM})$	$\mathbb{Q}^1, E(u_{FV})$	$\mathbb{Q}^2, E(u_{FV})$
1	-4.5230278474	-4.523568683883	-4.5230278425	-4.5233568683864
M	$\mathbb{Q}^1, J(u_{FEM})$	$\mathbb{Q}^2, J(u_{FEM})$	$\mathbb{Q}^1, J(u_{FV})$	$\mathbb{Q}^2, J(u_{FV})$
1	5.2434×10^{-6}	8.2205×10^{-8}	2.2928×10^{-14}	1.0261×10^{-13}

Table 5. Energy minimization and conservation indicator with $h = 2^{-9}$.

We present numerical experiments that verify our theoretical findings. We also stress the fact that our approximation of the solution has continuous tangential fluxes along primal element edges. The implementation of our method is simple and requires only coding tools used for classical conforming high-order finite element method plus the computation of fluxes of basis functions along control volumes boundaries (as in the classical low-order finite volume method).

Our formulation can be easily extended to a variety of cases where both high-order approximation and also conservative properties are desirable. For instance, we mention the case of flow problems in high-contrast multiscale porous media with sophisticated high-order discretization schemes, see [8]. We note that the analysis for this case and for other high-order approximation spaces is non-trivial as well as robust solvers are under investigation.

Acknowledgement:

Eduardo Abreu thanks in part by FAPESP 2016/23374-1 and CNPq Universal 445758/2014-7. Ciro Diaz thanks CAPES for a graduate fellowship. Marcus Sarkis thanks in part by nsf-mri 1337943 and nsf-mps 1522663.

References

[1] P. Grisvard, Elliptic problems in nonsmooth domains, Vol. 24 of Monographs and Studies in Mathematics, Pitman (Advanced Publishing Program), Boston, MA, 1985.
 [2] P. Bastian, A fully-coupled discontinuous Galerkin method for two-phase flow in porous media with discontinuous capillary pressure, Comput. Geosci. 18 (5) (2014) 779–796. doi:10.1007/s10596-014-9426-y. URL <http://dx.doi.org/10.1007/s10596-014-9426-y>
 [3] B. Andreianov, C. Cancès, Vanishing capillarity solutions of buckley–leverett equation with gravity in two-rocks medium, Computational Geosciences 17 (3) (2013) 551–572.
 [4] J. Douglas, Jr., F. Furtado, F. Pereira, On the numerical simulation of waterflooding of heterogeneous petroleum reservoirs, Comput. Geosci. 1 (2) (1997) 155–190. doi:10.1023/A:1011565228179. URL <http://dx.doi.org/10.1023/A:1011565228179>

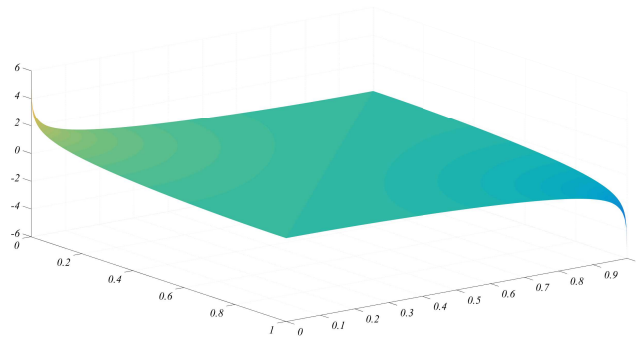


Figure 7. Plot of numerical solution for the problem with homogeneous Neumann boundary conditions and singular right hand side.

<i>FEM</i>		Q^1	Q^2
	L^1	1.8463	1.8707
	L^2	1.0000	1.0121
	$W^{1,1}$	0.8694	0.9983
<hr/>			
<i>FV</i>			
<i>FV</i> + λ	L^1	1.8490	1.8715
<i>FV</i> + λ	L^2	1.0000	1.0000
	$W^{1,1}$	0.8590	0.9977

Table 6. Values of L^1 , L^2 and $W^{1,1}$ error order of *FEM* and *FV* for the homogeneous Neumann boundary condition problem with singular forcing.

- [5] J. Dong, B. Rivière, A semi-implicit method for incompressible three-phase flow in porous media, *Comput. Geosci.* 20 (6) (2016) 1169–1184. doi:10.1007/s10596-016-9583-2.
URL <http://dx.doi.org/10.1007/s10596-016-9583-2>
- [6] E. Abreu, Numerical modelling of three-phase immiscible flow in heterogeneous porous media with gravitational effects, *Math. Comput. Simulation* 97 (2014) 234–259. doi:10.1016/j.matcom.2013.09.010.
URL <http://dx.doi.org/10.1016/j.matcom.2013.09.010>
- [7] E. Abreu, J. Douglas, Jr., F. Furtado, D. Marchesin, F. Pereira, Three-phase immiscible displacement in heterogeneous petroleum reservoirs, *Math. Comput. Simulation* 73 (1-4) (2006) 2–20. doi:10.1016/j.matcom.2006.06.018.
URL <http://dx.doi.org/10.1016/j.matcom.2006.06.018>
- [8] M. Presho, J. Galvis, A mass conservative generalized multiscale finite element method applied to two-phase flow in heterogeneous porous media, *J. Comput. Appl. Math.* 296 (2016) 376–388. doi:10.1016/j.cam.2015.10.003.
URL <http://dx.doi.org/10.1016/j.cam.2015.10.003>
- [9] Y. Efendiev, J. Galvis, T. Y. Hou, Generalized multiscale finite element methods (GMsFEM), *J. Comput. Phys.* 251 (2013) 116–135. doi:10.1016/j.jcp.2013.04.045.
URL <http://dx.doi.org/10.1016/j.jcp.2013.04.045>
- [10] Y. Efendiev, J. Galvis, X.-H. Wu, Multiscale finite element methods for high-contrast problems using local spectral basis functions, *J. Comput. Phys.* 230 (4) (2011) 937–955. doi:10.1016/j.jcp.2010.09.026.
URL <http://dx.doi.org/10.1016/j.jcp.2010.09.026>
- [11] J. Galvis, Y. Efendiev, Domain decomposition preconditioners for multiscale flows in high contrast media: reduced dimension coarse spaces, *Multiscale Model. Simul.* 8 (5) (2010) 1621–1644. doi:10.1137/100790112.
URL <http://dx.doi.org/10.1137/100790112>
- [12] J. Galvis, Y. Efendiev, Domain decomposition preconditioners for multiscale flows in high contrast media: reduced dimension coarse spaces, *Multiscale Model. Simul.* 8 (5) (2010) 1621–1644. doi:10.1137/100790112.
URL <http://dx.doi.org/10.1137/100790112>
- [13] L. Chen, A new class of high order finite volume methods for second order elliptic equations, *SIAM J. Numer. Anal.* 47 (6) (2010) 4021–4043. doi:10.1137/080720164.
URL <http://dx.doi.org/10.1137/080720164>
- [14] Z. Chen, J. Wu, Y. Xu, Higher-order finite volume methods for elliptic boundary value problems, *Adv. Comput. Math.* 37 (2) (2012) 191–253. doi:10.1007/s10444-011-9201-8.
URL <http://dx.doi.org/10.1007/s10444-011-9201-8>

<i>FEM</i>		Q^1	Q^2
	L^1	1.9999	3.0000
	L^2	1.9999	3.0000
	$W^{1,1}$	1.0000	2.0000
<i>FV</i>			
<i>FV</i> + λ	L^1	2.0000	3.0000
<i>FV</i> + λ	L^2	1.9999	3.0000
	$W^{1,1}$	1.0000	2.0000

Table 7. Values of L^1 , L^2 and $W^{1,1}$ error order of *FEM* and *FV* for the homogeneous Neumann boundary condition problem with smooth forcing.

- [15] Z. Chen, Y. Xu, Y. Zhang, A construction of higher-order finite volume methods, *Math. Comp.* 84 (292) (2015) 599–628. doi:10.1090/S0025-5718-2014-02881-0.
URL <http://dx.doi.org/10.1090/S0025-5718-2014-02881-0>
- [16] D. Cortinovis, P. Jenny, Iterative Galerkin-enriched multiscale finite-volume method, *J. Comput. Phys.* 277 (2014) 248–267. doi:10.1016/j.jcp.2014.08.019.
URL <http://dx.doi.org/10.1016/j.jcp.2014.08.019>
- [17] L. J. Durlofsky, A triangle based mixed finite element finite volume technique for modeling two phase flow through porous media, *Journal of Computational Physics* 105 (2) (1993) 252–266.
- [18] G. M. Homsy, Modeling fluid flow in oil reservoirs, *Ann. Rev. Mech.* 37 (205) 211–238.
- [19] M. Ghasemi, Y. Yang, E. Gildin, Y. R. Efendiev, V. M. Calo, Fast multiscale reservoir simulations using pod-deim model reduction, in: *SPE reservoir simulation symposium*, 2015.
- [20] J. Bear, A. H.-D. Cheng, *Modeling groundwater flow and contaminant transport*, Vol. 23, Springer Science & Business Media, 2010.
- [21] M. Benzi, G. H. Golub, J. Liesen, Numerical solution of saddle point problems, *Acta Numer.* 14 (2005) 1–137. doi:10.1017/S0962492904000212.
URL <http://dx.doi.org/10.1017/S0962492904000212>
- [22] S. C. Brenner, L. R. Scott, *The mathematical theory of finite element methods*, 3rd Edition, Vol. 15 of *Texts in Applied Mathematics*, Springer, New York, 2008. doi:10.1007/978-0-387-75934-0.
URL <http://dx.doi.org/10.1007/978-0-387-75934-0>
- [23] D. Braess, *Finite elements: Theory, fast solvers, and applications in solid mechanics*, Cambridge University Press, 2007.
- [24] P.-A. Raviart, J. M. Thomas, Primal hybrid finite element methods for 2nd order elliptic equations, *Math. Comp.* 31 (138) (1977) 391–413. doi:10.2307/2006423.
URL <http://dx.doi.org/10.2307/2006423>